Rheological performance of cementitious materials used in well cementing

Doctoral Thesis by

Helge Hodne

Thesis submitted in fulfilment of the requirements for the degree of

DOCTOR OF PHILOSOPHY
(Ph.D.)

University of Stavanger

Faculty of Science and Technology
Department of Petroleum Engineering

Stavanger July 6, 2007

University of Stavanger
NO-4036 Stavanger
NORWAY
www.uis.no

ISBN: 978-82-7644-334-9
ISSN: 1890-1387

Preface

The present dissertation comprises 10 papers published in the period from 2000 to 2007. Four of them are published as peer reviewed papers in journals and six are presented at conferences and published in the conference proceedings. The papers are preceded by a review. The papers are enumerated in a chronological order with respect to date of publication using Roman numerals. The Roman numerals have also been used when referring to these papers in the present review.

In Paper I a study of mixing energy and its effect on the rheological behaviour of cement suspensions, together with a comparison of testing methods, is presented.

In Paper II the effect of time and mixing energy is extended to also consider its effects on the zeta-potential of cement particles. The work presented in Paper I and II were a continuation of work presented in two earlier papers, one published in 1997 [1] and one in 1998 [2], originally intended to form a part of this thesis. However, due to changes taking place later in the course of the present study they have not been included as they were found to lie somewhat outside the scope of this work.

Paper III contains the verification of a calibration standard, a standard used when calibrating the AcoustoSizer used in Papers II and IV-VIII for measuring the zeta-potentials of cementitious particles.

Paper IV and V presents a study of rheological properties of cementitious suspensions used for high temperature oil well cementing. In Paper IV the effects of additives on the zeta-potentials are evaluated and collated with rheological data.

In Paper V the rheology and zeta-potentials of crystalline and amorphous silica are studied.

Paper VI comprises a rheological study concerning the effect of gypsum on clinker and its main constituents.

In Paper IX, the effect of shear on the removal of entrapped air in the aggregates

formed by the cement particles in the suspensions is studied.
The last three papers, Paper VII, VIII and X, are concerned with rheological modelling. In oil well cementing there is a need for being able to predict the rheological behaviour of the suspensions over a wide range of parameters, normally extending those of the standard laboratory testing methods. Thus, modelling is widely in use and in these papers a rather new model, up till now not much used for cementitious suspensions, is presented and evaluated. This is a model, proposed by Quemada [3] in 1998, that takes into account the inter-particle forces in concentrated suspensions.

Acknowledgments

The work presented in this dissertation has for the major part been carried out at the University of Stavanger, at the Department of Petroleum where I am employed as an assistant professor. Here the Department has provided me with excellent working conditions and I would like to thank all my colleagues for their patience and support.
The research that resulted in Paper III, was carried out at the University of Sydney, from July 1999 to June 2000. In Sydney I had the pleasure of working at the School of Chemistry under the guidance of associate professor James K. Beattie, and to whom I am very thankful.
My supervisor has been PhD Arild Saasen, formerly an associate professor at the Department, now an employee at Statoil ASA and lately also a professor II at the Department. I wish to express my sincere thanks to him for his continuous guidance and support during these years.
Finally I would like to thank my wife Helga for her support and patience. Without her I would never have started.

List of papers

The papers are referred to in the following review by their Roman numerals and copies are enclosed subsequently in the appendix.

I Hodne, H., Saasen, A., O'Hagan, A.B. and Wick, S.O., "Effects of time and shear energy on the rheological behaviour of oil well cement slurries," Cem. and Concr. Res., **30**, 1759-1766, (2000).

II Hodne, H. and Saasen, A., "The effect of the cement zeta potential and slurry conductivity on the consistency of oil well cement slurries," Cem. Concr. Res., **30**, 1767-1772, (2000).

III Hodne, H. and Beattie, J.K., "Verification of the Electroacoustic Calibration Standard: Comparison of the Dynamic Mobility of Silicododecamolybdate and Silicododecatungstate Acids and Salts", Langmuir, **17**, 3044-3046, (2001).

IV Hodne, H., Saasen, A. and Strand, S., " Rheological Properties of High Temperature Oil Well Cement Slurries", Annual Transactions The Nordic Rheology Society, **9**, 31-38, (2001).

V Hodne, H., Saasen, A., Håheim, S. and Ovesen, E., " Rheological Properties of High Temperature Silica Oil Well Slurries", Annual Transactions The Nordic Rheology Society, **10**, 51-55, (2002).

VI Hodne, H. and Saasen, A., "Rheological Properties of the Silica phases in Clinker Slurries", Annual Transactions The Nordic Rheology Society, **11**, 103-106, (2003).

VII Hodne, H. and Saasen, A., "Rheological Modelling of Cementitious Materials", Annual Transactions The Nordic Rheology Society, **12**, 109-113, (2004).

VIII Hodne, H., Saasen, A. and Pita, E., "Rheology of cementitious suspensions containing weighting agents", Annual Transactions The Nordic Rheology Society, **13**, 191-197, (2005).

IX Hodne, H., Falkeid, V. and Saasen, A., "The influence of entrapped air on rheological properties of cement suspensions in early state of hydration", Annual Transactions The Nordic Rheology Society, **14**, 103-106, (2006).

X Hodne, H., Galta, S. and Saasen, A., "Rheological modelling of cementitious materials using the Quemada model", Cem. and Concr. Res., **37**, 543-550, (2007).

Nomenclature

A	Hamaker constant	J
A	Aluminium oxide	Al_2O_3
Bc	Bearden units of consistency	
C	Compactness factor	
C	Interaction constant	Jm^6
C	Calcium oxide	CaO
°C	Temperature in degree Celsius or centigrade	
D	Distance between surfaces	m
DLVO	**D**erjaguin, **L**andau, **V**erway, **O**verbeek	
ESA	**E**lectro **S**onic **A**mplitude	
EVF	**E**ffective **V**olume **F**raction	
F	Iron oxide	Fe_2O_3
G	Inertia term	
HS	**H**ard **S**phere	
IF	**I**ndividual **F**locs	
K_s	Surface conductance of double layer	Sm^{-1}
K^∞	Conductance of liquid	Sm^{-1}
K-D	**K**rieger-**D**ougherty	
N	Number density of suspended particles	
$\overline{R}$	Mean radius of SU's, $\overline{R}(\Gamma)$	m
R_{eff}	Effective radius of an SU	m
S	Silica oxide	SiO_2
S	Structural variable, $S = \phi_A/\phi$	
S_{eq}	Structural variable in equilibrium	
S_0	Structural variable, $S_0 = \phi_{A0}/\phi$ when $\dot{\gamma} \rightarrow 0$	
S_∞	Structural variable, $S_\infty = \phi_{A\infty}/\phi$ when $\dot{\gamma} \rightarrow \infty$	
SEM	**S**canning **E**lectron **M**icroscopy	
SFA	**S**urface **F**orces **A**pparatus	
SG	**S**pecific **G**ravity	

SME	**S**pecific **M**ixing **E**nergy	J/kg
SU	**S**tructural **U**nit	
T	Absolute temperature	K
T	Torque	gcm
W_A	Attractive interaction potential	J
W_R	Repulsive interaction potential	J
W_S	Structural term	J
W_{tot}	Total interaction potential	J
Å	Ångström $= 10^{-8}$cm	
a	Diameter of particle or sphere	m
c	Unit concentration of the dispersed phase	
d	Distance between center of two particles or spheres	m
$d50$	Average diameter of particles	m
k	Consistency Index	Pas^n
n	Number of particles	
n	Power Law Index	
p	Exponent	
q	Exponent, $q = [\eta]\phi_m$	
r	Radius of particle or sphere	m
r_{eff}	Effective radius	m
t_A	Mean relaxation time for the aggregation of SU's	s
t_c	Characteristic time required for a dimensional homogeneity	s
t_D	Mean relaxation time for the destruction of SU's	s
t_{Ex}	Duration of experiment	s
u_d	Dynamic mobility	$\mathrm{m^2V^{-1}s^{-1}}$
u_E	Electrophoretic mobility	$\mathrm{m^2V^{-1}s^{-1}}$
w/c	Water cement ratio	
Γ	Shear variable, either $\Gamma = \sigma/\sigma_c$ or $\Gamma = \dot{\gamma}\ /\ \dot{\gamma}_c$	
α	The variable of the inertia term	
$\dot{\gamma}$	Shear rate	$\mathrm{s^{-1}}$
$\dot{\gamma}_c$	Characteristic shear rate	$\mathrm{s^{-1}}$
δ	Thickness of Stern layer	m
ε	Permittivity of liquid	$\mathrm{C^2J^{-1}m^{-1}}$
ε_p	Permittivity of particle	$\mathrm{C^2J^{-1}m^{-1}}$
ε_r	Relative permittivity or dielectric constant, $\varepsilon_r = \varepsilon/\varepsilon_0$	
ε_0	Permittivity of vacuum	$\mathrm{C^2J^{-1}m^{-1}}$
η	Viscosity	Pas
$[\eta]$	Intrinsic viscosity, dimensionless for suspensions	
η_F	Viscosity of suspending fluid	Pas

η_r	Relative viscosity,	$\eta_r = \eta/\eta_F$	
η_p	Plastic viscosity,		Pas
$\eta_{solution}$	Viscosity of solution		Pas
$\eta_{solvent}$	Viscosity of solvent		Pas
η_{sp}	Specific viscosity		
η_0	Limiting steady state viscosity as $\dot{\gamma} \rightarrow 0$		Pas
η_∞	Limiting steady state viscosity as $\dot{\gamma} \rightarrow \infty$		Pas
θ	Ratio between mean aggregation and destruction time of SU's, t_A/t_D		
κ	Inverse Debye length		m^{-1}
κ_A	Shear dependent kinetic constant of formation of SU's, $\kappa_A = t_A^{-1}$		s^{-1}
κ_D	Shear dependent kinetic constant of destruction of SU's, $\kappa_D = t_D^{-1}$		s^{-1}
λ	Enhanced conductivity		m^{-1}
ν	Kinematic viscosity		$\mathrm{m}^2\mathrm{s}^{-1}$
ζ	Zetapotential		mV
ρ	Number density		m^{-3}
ρ	Specific density		kgm^{-3}
$\rho_{\infty i}$	Ionic concentration of ion i in the bulk		m^{-3}
$\Delta\rho$	Specific density difference		kgm^{-3}
σ	Shearstress		Pa
σ_c	Characteristic shearstress		Pa
σ_y	Yield stress		Pa
ϕ	Packing fraction		
ϕ	Solid volume fraction		
ϕ	Volume fraction		
ϕ_A	Volume fraction of SU's		
ϕ_{Aeff}	Effective volume fraction of SU's		
ϕ_{A0}	Volume fraction of particles contained in all the SUs when $\dot{\gamma} \rightarrow 0$		
$\phi_{A\infty}$	Volume fraction of particles contained in all the SUs when $\dot{\gamma} \rightarrow \infty$		
ϕ_{eff}	Effective volume fraction of IFs and SUs		
ϕ_I	Volume fraction of IF's		
ϕ_m	Maximum volume packing fraction		
ϕ_{PK}	Effective maximum packing fraction		
ϕ_{RCP}	Random close packing fraction		
ϕ_0	Limiting maximum volume packing fraction as $\dot{\gamma} \rightarrow 0$		
ϕ_∞	Limiting maximum volume packing fraction as $\dot{\gamma} \rightarrow \infty$		
φ	Mean compactness of SU's		

φ_n	Compactness of SU's	
χ	Rheological index, $\chi(\phi)$	
ψ	Electrostatic surface potential	V
ψ_d	Electrostatic potential in the Stern plane	V
ψ_0	Electrostatic potential at the particle surface	V
ω	Frequency of alternating electric field	s^{-1}
$\omega^{'}$	Influence of liquid on frequency	m^{-1}

Prefix symbols

M	Mega, 10^6
m	Milli, 10^{-3}
μ	Micro, 10^{-6}
n	Nano, 10^{-9}

Contents

Chapter 1

Introduction

1.1 Well cementing

Primary well cementing is one of the most important operations performed on an oil or gas well. During the cementing operation, a suspension consisting mainly of water, cement and performance controlling chemicals is pumped down into the well and placed at the cementing interval between the casing and the formation and left to cure. The purpose of this operation is to anchor the casing to the formation and to achieve zonal isolation down in the well. The anchoring of the casing is normally achieved but the challenge is to obtain a complete zonal isolation. This implies that a hydraulic seal must be obtained between cement and casing as well as between cement and formation in the cemented interval. When failing to obtain such a seal the result is a well that never will reach its full potential as a gas or oil producer.
The most common principle used for primary well cementing is the two plug method. When the well has been drilled to the right depth, the drill-pipe is removed and a casing or liner, with the appropriate diameter is lowered down into the well. During this operation the well must at all times be filled with drilling fluid on the outside of the casing or liner. A constant hydrostatic pressure in the well is needed both to hinder the wall in weak zones from collapsing into the well and to balance the fluid pressure of the formation and thus prevent unwanted production of formation fluids. When cementing, two plugs are placed inside the casing or liner with the amount of cement to be used placed in between. During pumping down the well the plugs keep the cement and the drilling fluids separated. When the cement reaches the end of the casing or liner the leading plug brakes and the cement is pumped through the plug, around the casing or

liner shoe, and up on the outside between the casing or liner, and the formation. When the tail-plug reaches the bottom of the casing or liner, and essentially all the cement is in the annulus, the pumping is stopped and the cement is left to cure.
Replacing drilling fluid with cement between casing and formation is considered to be the most critical part of the cementing job. The more efficient the removal of the drilling fluid is, the better the bonding between cement and casing and cement and formation will be. Much effort is put into obtaining a good bondage and various types of remedies, both mechanical and chemical are in use. The properties of the cement suspension, i.e. density, viscosity and pumping velocity, play an important part and contributes significantly to the success of the cementing job.
Rheology is defined as the science of deformation and flow of materials in response to applied stresses. For our purpose it is defined through equations giving the relation between shear rate and shear stress for concentrated suspensions of cementitious materials. These are suspensions that rheologically behave mostly in a non-Newtonian way, i.e. the deformation and flow of the suspensions depend on the applied stress in a non-linear way.
Being able to predict the rheological behaviour of the cementitious suspensions when pumped down the well, has always been a challenge. The understanding of the rheology of cementitious suspensions is important for the design, execution and evaluation of a primary cementing job. Our understanding is based on measurements carried out in the laboratories and the task is to relate these data, using rheological models, to the conditions experienced by the suspensions down in the well in order to predict the success of the cementing job. In the present dissertation a rheological model named the Quemada model [3] has been used for describing the behaviour of cementitious suspensions. A model hitherto not commonly used in the drilling industry.

Chapter 2

Objective

The rheological behaviour of suspensions made up of cementitious materials and used for oil well cementing is to a great extent governed by the initial mixing conditions combined with the forces acting between the particles. This will also govern the time dependent rheology of the suspensions and thus their ability to fully replace other fluids in the cementing interval.
The objective of the present study has been to achieve a better understanding of the factors involved. This is essential for the interpretation of the rheological measurements made in the laboratory which again form the basis for the predictions given for the behaviour of the cementitious suspensions when pumped down into the well. Further, the objective has been to evaluate the performance of the rheological model proposed by Quemada [3] in 1998 for concentrated suspensions, on the performance of cementitious materials used for well cementing. This is a model that tries to incorporate the influence of inter-particle forces on the rheological behaviour of suspensions, a model not commonly used for predicting the behaviour of cementitious suspensions.

Chapter 3

Materials, mixing and measuring methods

3.1 Cementitious materials

Materials used for cementing purposes are commonly called cementitious materials. Cementitious materials are the most widely used materials for building and construction works in the world. Materials that belong to this group include various types of cements, fly ashes, silica fumes, blast furnace slag and some aplites. They are mainly more or less amorphous oxides and have in common the ability to react with water and solidify under certain conditions.
The variations in pressure and temperature encountered in oil wells necessitates the use of various types of cement, often in combination with other types of materials in order to achieve the required properties. In the present study we have tested various types of cement, its main constituents and also cement in combination with both water reactive and rather non-reactive materials; all used for cementing of oil wells. Here follows a brief presentation of the materials used in this study.

3.1.1 Clinker

Clinker is the main ingredient of Portland cement. When producing clinker for Portland cement, various ground oxides containing mostly calcium and silica with minor contents of alumina and iron, are fed into a heating oven where they partly melt and combine. The product exiting the oven is termed cement clinker. The four main components of this clinker are tricalcium silicate

(C_3S), dicalcium silicate (C_2S), tricalcium aluminate (C_3A) and tetracalcium aluminoferrite (C_4AF). The term in brackets is a conventional special notation frequently used by cement chemists [4] where C=CaO, S=SiO_2, A=Al_2O_3 and F=Fe_2O_3.
The final step in making Portland cement is to grind the clinker together with a sulphate source, normally gypsum. As the four clinker components reacts differently with water, i.e. their hydration time differs, the adding of 3-5% of gypsum [5] delays the most rapid hydrations taking place between C_3A and water. Thus, the adding of gypsum leaves us with a cement that can be mixed with water and where the time before setting is sufficient for the placement of the cement suspension in the well.
The main constituents of the clinker are the silica phases with C_3S concentrations as high as 70%. Paper VI comprises a study of the rheological behaviour of triclinic and monoclinic C_3S, with the effect of adding gypsum. Clinker was also used in Paper VII as a suspension subjected to rheological modelling.

3.1.2 Cement

Two types of cement are normally in use for well cementing in the North Sea. One is a normal Portland cement type termed Class A by API [6]. The other is a modified Portland cement termed Class G. The Class A cement is intended for use from surface down to 1830 m when no special properties are required. According to API [6] the Class G is a sulfate-resistent cement intended for use as a basic well cement from surface down to 2440 m. However, this type of cement, together with additives, are used for all depths in the North Sea. The main differences between the two types of cement are that the Class G has a lover content of C_3A and a higher content of C_4AF, making it more sulfate-resistant, and that the Class G cement has a lower surface area than that of the Class A cement. The presence of a lower surface area means that the Class G cement has a coarser particle size distribution resulting in longer setting times compared to that of the Class A cement.
Both cements were used for our work presented in Paper I, where the Class A type cement was named P-30. Further, suspensions made of neat Class G cement has been used for measurements in all our papers and thus forming a reference throughout our work.

3.1.3 Silica

The silica used in cementing is defined as pozzolans, i.e. silicous material which in itself possesses little or no cementitious value but when added as small parti-

cles and in the presence of water will react chemically with calcium hydroxide at ordinary temperatures to form compounds possessing cementitious properties [7].
Two types of silica, i.e. crystalline silica flour and amorphous micro silica, are used in well cementing either as extenders or most frequently for the prevention of strength retrogression when encountering high temperatures in the cementing interval, or where the later production of oil leads to high temperatures. While the crystalline silica is produced from natural mineral deposits, the amorphous micro silica, or silica fume, is a byproduct from the metal melting industry.
The effect on the rheology of cement suspensions when adding silica were the subject for investigation in Paper IV and V and a micro silica suspension was also used for rheological modelling in Paper VII. The result of this modelling is presented in Sect. 6.3.4.

3.1.4 Manganese tetra oxide

For well cementing, where higher density cement suspensions are needed weighting agents are added. Manganese tetra oxide, Mn_3O_4, is commonly used as a weighting agent in cements and drilling fluids. It has a specific gravity of 4.8 which is slightly higher than the 4.2 of Barite, the most common used weighting agent for drilling fluids. The manganese tetra oxide used for our experiments was delivered by Elkem ASA under the trading name Micromax®, and for short this name will be used in the present work. Micromax is a byproduct from the metal melting industry. It is condensed fume from the blast furnace process. The particle size distribution is rather narrow having a d50 of 0.4 μm This is small compared with that normally found for Barite. Micromax is thus used when it is important to avoid larger particles in the fluids. When mixed with water and cement it is found to be almost inert and insoluble.
The rheological properties of cement suspensions containing Micromax were investigated in Paper VIII and X. In these papers the premixed suspensions where also tested for rheological modelling.

3.2 Standard mixing procedure for laboratory preparation of well cements

To obtain homogenous and pumpable suspensions of cementitious materials in water, a considerable amount of energy has to be used in the mixing process to properly disperse the particles. The variations in mixing energy and its influence on the various properties of the cement suspensions are well documented both

for suspensions used in the building industry [8, 9] and for oil well cementing [10, 11, 12, 13].
The mixing and testing of cementitious suspensions for use in oil well cementing is carried out in accordance with API Standards [6, 14]. The standard procedure involves the initial use of a high speed mixer, described in Sect. 3.2.1, whereafter the suspension is placed in an atmospheric consistometer, described in Sect. 3.2.2. The duration of this preparation process, approximately 22 minutes, is expected to be sufficient for the the cement to reach the induction period [5]. This means that the testing takes place during a period of low chemical activity, and thus, negligible variations of the testing results due to hydration is expected. It is during this induction period that the pumping of the cement suspension down into the well takes place.

3.2.1 The high speed mixing

The high speed mixer, as specified by API [6, 14], to be used for the initial mixing of cement suspensions prior to any laboratory testing, shall be of a two speed propeller-type capable of rotating at 4000 r.p.m. or greater under no load on slow speed, and 12000 r.p.m. or greater under no load on high speed. The propeller blade shall be made of corrosion-resistant metal and it is recommended to replace the blade when a 10% loss of weight is registered. The volume of the mixing container shall be approximately 1 liter.
The above is a description of a standard kitchen utility mixer called a Warring Commercial Blender and it is also the mixer we have used when preparing our samples.
The mixing procedure in the high speed mixer consist of an initial period at 4000 r.p.m., lasting 15 seconds, during which the cement is added to the water, whereafter the speed is increased to 12000 r.p.m. for a period of 35 seconds.

3.2.2 The atmospheric consistometer

The atmospheric consistometer is a dynamic testing device. It is described by API [6, 14] and it is in principle a rather slow rotating mixer able to mix a volume of approximately 600 cm^3. In the consistometer the suspension container rotates while the paddle is held in a fixed position. The torque needed to hold the paddle still in the rotating suspension is measured and is used to determine the time interval during which the suspension is defined as pumpable. The end of this interval is said to be reached when a value of 30 Bearden units of consistency (Bc) is measured. The Bc value is dimensionless. However, when calibrating the consistometer in accordance with API [6, 14] a torque of 66.6

10^{-3}Nm (mNm) is found to correspond with the value of 30 Bc:

$$T = 78.2 + 20.02\text{Bc} \tag{3.1}$$

where T is the torque in gcm and Bc is the Bearden units of consistency.
Note that in Paper I and II, due to a miss-interpretation, the value of 42.2 mNm was reported as being equivalent to 30 Bc, the times reported for the suspensions to reach 30 Bc in these papers are somewhat shorter than the true values. However, all consistency measurements are shown in our figures as torque v.s. time. Therefore our conclusions should not be influenced by this error. In Paper IV the correct torque value was reported for 30 Bc.

Chapter 4

Inter-particle forces and measurements

4.1 Inter-particle forces

Inter-particle forces to a large degree dictates the time and shear dependent rheological behaviour of suspensions. In the present work studies of the inter-particle forces in cementitious suspensions are used to obtain a better understanding of their influence on the shear dependent development of the viscosity. The inter-particle forces between particles suspended in an electrolyte, such as water, are mainly of electrostatic origin. We discern between two types, the attractive van der Waals forces and repulsive electrostatic double layer forces.

4.1.1 Attractive forces - van der Waals forces

Van der Waals interaction forces are omnipresent. They are of essentially electrostatic origin, arising from the dipole field of an atom "reflected back" by a second atom which is being polarized by this field. They are rather short ranged compared with electrostatic double layer forces, and are largely insensitive to variations in electrolyte concentration and pH so they can be considered as fixed in a first approximation [15].
Whereas the non-retarded van der Waals energy between atoms and molecules is of short range, having an inverse sixth-power distance dependence, the van der Waals energy between large extended bodies decays more slowly with distance, D, between their surfaces. Calculated on the basis of pairwise additivity by using the Hamaker summation method [15], the distance dependence is found

to be $1/D$ between a sphere and a flat surface and $1/D^2$ between two planar surfaces. According to Hunter [16], the non-retarded attractive interaction potential between two spherical particles of different size in vacuum can be written as:

$$W_A(r) = -\frac{A}{6}\left[\frac{2r_1r_2}{d^2-(r_1+r_2)^2} + \frac{2r_1r_2}{d^2+(r_1-r_2)^2} + \ln\left(\frac{\mathrm{d}^2-(\mathrm{r}_1+\mathrm{r}_2)^2}{\mathrm{d}^2-(\mathrm{r}_1-\mathrm{r}_2)^2}\right)\right] \quad (4.1)$$

Here A is the Hamaker constant, $A = \pi^2 C\rho_1\rho_2$ where C is the interaction constant, ρ_1 and ρ_2 the number densities of particle 1 and 2 respectively, r_1 and r_2 the radi of particle 1 and 2, and d is the distance between the center of the two particles. When the diameter, a, of the particles is much bigger than the distance between their surfaces, $a_1, a_2 >> D$, the Derjaguin approximation [16] can be used. The expression for the non-retarded van der Waals interaction free energy then reduces to [15][16]:

$$W_A(D) = -\frac{A}{6D}\frac{r_1r_2}{(r_1+r_2)} \quad (4.2)$$

here $D = d - (r_1 + r_2)$.
When the particles are surrounded by an interacting fluid, the van der Waals interaction energy calculated by the Hamaker method, is of limited use. Although the distance dependence of the force is not changed, the fluid can change the Hamaker constant as much as by one or even two orders of magnitude [16]. To generalize, like particles will still always attract when submerged in a fluid, but unequal particles may either attract or repel each other.

4.1.2 Repulsive forces - electrostatic double layer

Most particles acquire a surface electric charge when brought into contact with a polar medium, such as water. The possible charging mechanisms being ionization, ion adsorption and ion dissolution [17]. This surface charge attracts ions of opposite charge, counter-ions, in the surrounding medium and repel ions of same charge, co-ions. This leads to the formation of an electric double-layer made up of the charged surface and adjacent to this a more or less neutralizing layer of counter-ions in excess over co-ions, distributed in a diffuse manner in the polar medium, as shown in Fig. 4.1. The electrostatic double-layer interaction results in a repulsive force between particles of the same type. The double-layer interaction between surfaces or particles are sensitive to both variations in electrolyte concentration and pH, and decays exponentially with distance.

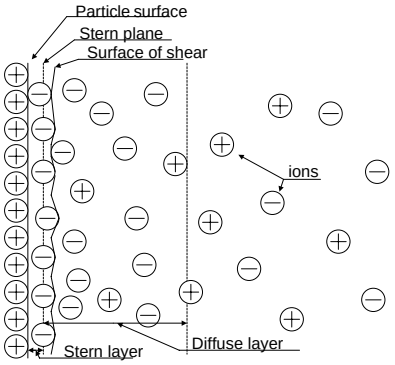

Figure 4.1: *Schematic representation of the structure of the electric double layer according to Stern's theory. The double layer consist of a fixed and a diffuse layer.*

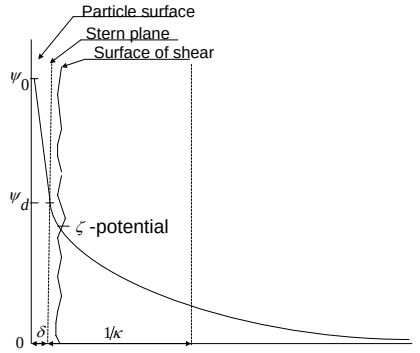

Figure 4.2: *Potential decrease as a function of distance from the particle surface. At the distance δ, there is a fixed layer of negative charge insufficient to balance the positive charge on the particle.*

The characteristic decay length, $1/\kappa$, as shown in Fig. 4.2, is called the Debye length, where κ has the unit of m^{-1}.
For two identical spherical particles of radius r having a low potential and for $r\kappa >> 1$, which is normally the case for cement particles, Hunter [16] gives the following approximation for the repulsive potential of the double layer:

$$W_R = 2\pi r \varepsilon_r \varepsilon_0 \psi^2 \ln\left[1 + \frac{1}{\mathrm{e}^{\kappa(\mathrm{d}-2\mathrm{r})}}\right] \tag{4.3}$$

Here ε_r is the relative permittivity of the fluid between the particles, often called the dielectric constant of the fluid, ε_0 is the permittivity of vacuum, ψ is the electrostatic surface potential, and $(d - 2r)$ is the separation of the particle surfaces.

4.1.3 Summation of forces - the DLVO theory

The summation of the attractive van der Waals and the repulsive double-layer forces is the essence of the DLVO theory, named after Derjaguin, Landau, Verwey and Overbeek. The total DLVO forces between two surfaces in an electrolyte can be measured by the use of a Surface Forces Apparatus (SFA) [15]. The SFA

measures directly the interaction forces between smooth surfaces in liquids down to the Ångström level, 10 nm. According to Israelachvili [15] the DLVO theory has been confirmed by measurements, done on mica surfaces, to a remarkable degree of accuracy at all separations, even down to 2% of κ^{-1}. This indicates that the DLVO theory is basically sound. Furthermore, the surface potential inferred from the magnitude of the double-layer forces in these measurements, agree within 10 mV with potentials measured independently on isolated mica surfaces by the method of electrophoresis.
By summation of the forces we get the total interaction potential between the particles:

$$W_{tot} = W_A + W_R \tag{4.4}$$

The interaction between the van der Waals forces and the double-layer forces can give rise to three different states regarding the particles in a suspension, depending on the ionic strength of the bulk solution:

i) Dispersed; At low ionic strength and high surface potentials we get a stable dispersion.

ii) Flocculated; At moderate ionic strength and medium to low surface potentials the suspension will tend to flocculate.

iii) Coagulated; At high ionic concentrations and relatively low surface potentials the particles coagulate.

Hunter [16] reports that experimental investigations of the coagulation properties of a wide range of colloidal solutions suggest that not all systems can be explained using the DLVO theory and that an extra, so-called structural, term W_S, must be included in Eq. 4.4. This W_S term can either be repulsive or attractive and is said to have influence on the total interaction when the distance, D between the surfaces is less than approximately 10 nm, arising because of the influence of a surface on adjacent solvent layers. Early evidence for the existence of this structural term came from the observations that some colloids (e.g. silica) could not be coagulated even at very high electrolyte concentrations, where the double layer should be completely compressed. Also, the phenomenon of re-dispersal of coagulated particles by dilution of the electrolyte cannot be explained by the simple DLVO theory. At present, the lack of an adequate theory for the structure of water prevents the theoretical evaluation of the important W_S term.

4.2 Measuring inter-particle forces

For cementitious particles the measurement of the total DLVO forces is rather complicated. It is not possible for these particles to maintain a smooth surface in water, as the surfaces react with the water, forming a double layer. This double layer, due to a continuous ongoing reaction between the particles and water, is never in static equilibrium with the surroundings. Ions from different parts of the particle surface continously dissolve into the water through the double layer at various rates and hydration products and ions precipitates from the surrounding water through the double layer and adhere to the particle surface. However, during the induction period and at the later phases the chemical reactions in the cementitious suspensions are rather slow, and treating the suspension as in equilibrium has shown to be successful [18]. This allows for measuring the double layer forces of the particles.

4.2.1 Measuring double-layer forces or zeta-potential

In general, surface charge of oxide systems can be measured [19] by titration with acid or base. This is based on the assumption that the only mechanism for removing OH^- or H^+ -ions from the solution is the adsorption of a hydroxyl ion or a proton or the removal of that very same from the surface. Although cementitious particles are to be considered as mainly oxides, the above method can not be used. The surface charge of cementitious (and many other) particles is not only due to the dissociation of surface groups. Also ions are readily dissolved from the surface when water is added. Therefore we are not able to estimate the surface charge of cementitious particles with a very high accuracy. But even if we could, it might be of little help in predicting the colloidal behaviour [19]. What is of interest is the effective charge, or the charge experienced by another approaching particle. This is what will determine the interaction between the particles. Ideally we would like to determine the electrostatic potential at the beginning of the diffuse part of the double layer [19], ψ_d, as shown in Fig. 4.2. In practice it can usually only be approximated by the measurement of the electrokinetic- or zeta-potential (ζ-potential), which is a measure of the potential in the plane of shear. Thus, no direct information is given about the potentials at the surface or in the Stern plane, which is situated about one hydrated ion radius from the surface, although the Stern potential is probably only slightly greater than the measured zeta-potential [19].

4.2.2 Electrokinetics

There are four electrokinetic phenomena that can be used to obtain the zeta-potential:

i) Electrophoresis, where a charged particle or surface is forced to move in a stationary liquid by an applied electric field.

ii) Electro-osmosis, where the liquid is forced to move relative to a charged surface by an applied electric field.

iii) Streaming potential, where an electric field is created when a liquid is forced to move past a stationary charged surface.

iv) Sedimentation potential, where an electric field is created when charged particles move relative to a stationary liquid.

We see from the above descriptions that sedimentation potential is the opposite of electrophoresis and streaming potential is the opposite of electro-osmosis. Here only the basis for obtaining the zeta-potential by electrophoresis or micro-electrophoresis as it often is called, will be looked into as this is the technique most in use for zeta-potential measurements of cementitious particles. It also forms the basis for the measuring technique used in this dissertation.

4.2.3 Electrophoresis or micro-electrophoresis

In electrophoresis the charged particle is forced to move in a stationary liquid by an applied electric field. When measuring the speed of the particles along the electric field-lines a microscope is often used, and thus the name micro-electrophoresis. This technique requires diluted suspensions. From the measured speed of the particles and the applied electric field the zeta-potential can be calculated.
Starting with Smoluchowski's solution to the electrophoretic problem [19] in which he regarded the liquid as fixed and changed the coordinate system from the solid surface to the liquid, and where the double layer thickness of the particle is thin compared to its radius, $r\kappa >> 1$, the following equation can be used to calculate the zeta-potential:

$$u_E = \frac{\varepsilon\zeta}{\eta} \tag{4.5}$$

Here u_E is the electrophoretic mobility, ε is the permittivity of the liquid, ζ is the zeta-potential, and η is the viscosity of the liquid. So for calculating the

zeta-potential one measures the speed of the particle and then divides it by the applied electric field to obtain its mobility.
For solving the electrophoretic problem for very thick double layers, $r\kappa << 1$, Hückle's equation [19] can be used:

$$u_E = \frac{2\varepsilon\zeta}{3\eta} \tag{4.6}$$

Eq. 4.5 and 4.6 were later combined by Henry [19] to give the following equation:

$$u_E = \left(\frac{2\varepsilon\zeta}{3\eta}\right) f(r\kappa) \tag{4.7}$$

In Eq. 4.7 the function f is introduced, which varies smoothly from 1 to 1.5 as $r\kappa$ varies from 0 to ∞. Eq. 4.7 is valid for zeta-potentials less than 25 mV.

The electrophoretic phenomenon described in this section to some extent founds the basis for the understanding and the theoretical development of electroacoustics which is described in the next section. Electroacoustics is also the technique used for measuring zeta-potentials of cementitious particles in the work presented here.

4.2.4 Electroacoustics

In contrast to electrophoresis where a direct voltage field is used to move the particles, electroacoustics apply an alternating voltage to the particle suspensions. This makes the particles move back and forth at a velocity depending on their size, their zeta-potential and the frequency of the applied field. As long as there is a difference in the specific density of the particles from that of the surrounding liquid, this back and forth movement results in a net mass transfer, which again results in the generation of a sound wave called the electrokinetic sonic amplitude or ESA effect. These sound waves, or electroacoustic waves can be measured and thus, we obtain a frequency dependent electrophoretic movement, or dynamic mobility, of the particles. These measurements, in contrast to the electrophoretic, are not constrained to dilute suspensions. From the dynamic mobility spectrum it is also possible to obtain the size distribution as well as the zeta-potential of the particles.
For dilute suspensions, approximately less than 4% by volume [20], of spherical particles having a thin double layer O'Brien [21] has shown that the dynamic

mobility is given by:

$$u_d = \frac{2\varepsilon\zeta}{3\eta} G\left(\frac{\omega d^2}{\nu}\right)\left(1 + f(\lambda\omega`)\right) \tag{4.8}$$

where

$$G(\alpha) = \frac{1 + (1+i)\sqrt{\frac{\alpha}{2}}}{1 + (1+i)\sqrt{\frac{\alpha}{2} + i\frac{\alpha}{9}\left(3 + 2\frac{\Delta\rho}{\rho}\right)}} \tag{4.9}$$

and

$$f(\lambda\omega`) = \frac{1 + i\omega` - \left(2\lambda + i\omega`\frac{\varepsilon_p}{\varepsilon}\right)}{2(1 + i\omega`) + \left(2\lambda + i\omega`\frac{\varepsilon_p}{\varepsilon}\right)} \tag{4.10}$$

where $\alpha = \frac{\omega\rho a^2}{\eta}$, $\lambda = \frac{K_s}{K^\infty a}$ and $\omega` = \frac{\omega\varepsilon}{K^\infty}$.

The $1 + f$ factor in Eq. 4.8 is proportional to the tangential electric field at the particle surface. This is the component of the electric field that generates the electrophoretic movement. As can be seen from Eq. 4.10, f depends on ε_p, the permittivity of the particle, ε, the permittivity of the liquid, K_s, the surface conductance of the double layer, K^∞, the conductance of the liquid, a, the diameter of the particle and ω, the frequency of the applied field. The parameter λ represents the enhanced conductivity due to the double layer at the particle surface. However, for thin double layer and relatively low zeta potential systems (as for cement particles) the surface conductivity has a negligible effect. Also, for water-based suspensions, the ratio $\varepsilon_p/\varepsilon$ is usually small and thus, Eq. 4.10 is reduced to $f = 0.5$. So the dynamic mobility defined in Eq. 4.8, can be given by a modified Smoluchowski equation:

$$u_d = \left(\frac{\varepsilon\zeta}{\eta}\right) G(\alpha) \tag{4.11}$$

The factor $G(\alpha)$ defined in Eq. 4.9, called the inertia term, represents the effect of inertia forces on the dynamic mobility and it is most strongly influenced

by the particle size a. It is also a function of ω, the frequency of the applied alternating electric field having an $\exp(i\omega t)$ variation; $\Delta\rho$, the specific density difference between the particle and the liquid; ρ, the specific liquid density and η, the viscosity of the liquid.
The G factor is a complex quantity and has a magnitude of unity and a phase angle of zero at low frequencies. As the frequency rises the magnitude of G falls monotonically to zero and the phase angle increases to a maximum value of 45°. This is the principal effect used in the particle sizing process. Thus, at low frequencies the particle size cannot be obtained, only the zeta potential. At higher frequencies the inertia of the particles becomes significant while the magnitude of the dynamic mobility, u_d, drops. The particle motion then begins to lag behind the applied field. Both the magnitude and the phase lag depends on the particle size such that a measurement of u_d can be used for getting size as well as zeta potential in the appropriate frequency regime.

4.2.5 The electroacoustic apparatus

The instrument used for our measurements of the zeta-potential is called an AcoustoSizer. The frequency range chosen for this instrument is 0.3 - 11 MHz allowing for sizing of particles in the range from 0.1 to 10 μm in diameter. The sizing is based on a log normal distribution model. For smaller particles the inertia forces are too small to allow sizing, only the zeta-potential of the particles can be determined. When the particle size distribution model of the AcoustoSizer fails to converge no zeta-potential value based on the dynamic mobility measurements is available. However, the measured mobility at 0.3 MHz can be used in Eq. 4.8 to obtain a zeta-potential (then $G = 1$ and $f = 0.5$ in Eq. 4.8 and thus Eq. 4.8 = Eq. 4.5). This is called the Smoluchowski zeta-potential in the terminology used in the AcoustoSizer manual [22]. The dynamic mobility measured at the lowest frequency of 0.3 MHz has been chosen for this purpose as this mobility resembles closest to the mobility obtained using direct voltage in an electrophoretic measurement.
According to Hunter [20] general equations for all particle concentrations of arbitrary density have not been found yet. Thus, for concentrated suspensions the AcoustoSizer uses a semi-empirical method to correct for concentration effects, based on the behaviour of common oxide systems.

4.2.6 Calibrating the AcoustoSizer

The sample cell of the AcoustoSizer has a volume of approximately 400 ml. It is equipped with an overhead propeller type mixer, so the sample can be agitated. This is useful for suspensions where the particles otherwise would tend to sediment during measurement. The cell also has probes to measure temperature, conductivity and pH. Furthermore, four thermally conducting ceramic rods immersed in the suspension provide temperature adjustment.
The instrument is calibrated at each frequency of measurement to account for the frequency dependence of the electronics and the physical components. The calibrating fluid used is a solution of the silicododecatungstate salt, KSiW. This was chosen as the quantities of this solution, that determine the ESA signal, can be independently evaluated from the literature and hence, an absolute determination of the zeta-potential of colloidal suspensions could be made with the AcoustoSizer once the instrument had been properly calibrated with this electrolyte.
In Paper III, working with a prototype of the AcoustoSizer-II model, we were able to verify the calibration standard in a study where we compared the dynamic mobility of silicododecamolybdate with that of silicododecatungstate, both their acids and their salts.

Chapter 5

Measuring and modelling rheological properties

5.1 Measuring rheological properties

The recommended equipment and methods for measuring the rheology of cementitious suspensions used for oil well cementing are given by API [6, 14]. Here it is required that the measurements are to be carried out by the use of a rotational viscometer equipped with two concentric measuring cylinders. The sample to be measured is confined between the two concentric cylinders and the width of the gap between the cylinders should be at least 10 times the diameter of the biggest particles found in the suspension. The surfaces of the cylinders are to be smooth.

5.1.1 Rheometers used

Two rheometers have been used in the present study. One was a CHAN 35 viscometer which was used for the rheological measurements presented in Paper I and VIII. This is a viscometer that meets the specifications given by API [6, 14] for measuring the rheology of cementitious suspensions. The API specifications gives that the inside diameter of the rotating sleeve should be 36.83 mm and that the diameter of the static bob should be 34.49 mm. The bob should be formed as a closed cylinder having a flat base and tapered top with a cone semi-angle of 60°. The cylinder length of the bob is 38 mm. Both cylinder and bob were equipped with a smooth surface for our measurements. The measuring gap between the bob and the sleeve is 1.17 mm. When comparing the size of the

gap with the diameter of the largest particles found in cement, given to be less than 100 μm [5], we find that this satisfies the recommendations given by API [14], and stated under Sect. 5.1.
The other rheometer used for our measurements was a Physica UDS 200 equipped with a concentric cylinder configuration named Z3DIN. In this instrument the bob is rotating and the measuring cup which also forms the outer sleeve is static. The diameter of the bob is 25 mm and the diameter of the sample cup is 27.11 mm. This gives a measuring gap of 1.055 mm, which also is found to satisfy the recommendations given by API [14]. The length of the measuring gap is 37.5 mm and the bob has the form of a closed cylinder with a flat top and a tapered bottom with a cone angle of 120°. This configuration having a smooth surface was used for our rheological measurements presented in Paper IV, V, VI, VII and IX. In Paper X we used a bob with a roughened surface but otherwise having the same dimensions as mentioned above.

5.2 Rheological modelling of complex fluids

The term complex fluids is widely used to describe fluids like concentrated suspensions i.e. fluids that have a shear dependent behaviour. These fluids often show a shear thinning behaviour when going from low to moderate shear rates followed by a shear thickening behaviour at higher shear rates. Concentrated suspensions of cementitious particles often show such a complex behaviour. However, for our experiments any high shear rates resulting in a shear thickening behaviour was not used.
The simplest rheological models describing the behaviour of suspensions of particles in Newtonian fluids, consider the suspensions to be diluted and the particles to be non-interacting hard spheres, HS, of even size. Such a model is given by the well known Einstein equation [23]:

$$\eta = \eta_F(1 + 2.5\phi) \tag{5.1}$$

Here η is the viscosity of the suspension, η_F is the viscosity of the suspending fluid and ϕ the solid volume fraction.
A model that has been found to be suitable for describing the behaviour of concentrated suspensions of both spherical and non-spherical particles is that given by the Krieger-Dougherty equation , K-D, [23]:

$$\eta = \eta_F\left(1 - \frac{\phi}{\phi_m}\right)^{-q} \tag{5.2}$$

Here ϕ_m is the maximum packing fraction and $q = [\eta]\phi_m$, where $[\eta]$ is the intrinsic viscosity. The intrinsic viscosity is dimensionless for suspensions, and it is the limiting value of the reduced viscosity as the concentration approaches zero. The reduced viscosity being the specific viscosity per unit concentration, c, of the solute or the dispersed phase which gives the relation:

$$[\eta] = \lim_{c \to 0} \left(\frac{\eta_{sp}}{c} \right) \tag{5.3}$$

The specific viscosity, η_{sp}, is the difference between the viscosity of a solution or dispersion and that of the solvent or continuous phase, divided by the viscosity of the solvent or the continuous phase:

$$\eta_{sp} = \frac{\eta_{solution} - \eta_{solvent}}{\eta_{solvent}} = \frac{\eta - \eta_F}{\eta_F} = \eta_r - 1 \tag{5.4}$$

In which the relative viscosity, η_r, is the ratio of the viscosity of the solution to the viscosity of the pure solvent.
The relation between Eq. 5.2 and Eq. 5.1 is given by the binomial theorem [24] where an expression written as Eq. 5.2 can be said to belong to a family of the type $(1-b)^{-a}$. This expression can be expanded into an endless series of terms starting as follows: $1+ab+\frac{1}{2}(a^2+a)b^2+....$ To apply this expansion to Eq. 5.2 we set $b = \frac{\phi}{\phi_m}$ and $a = q$. Then Eq. 5.2 becomes: $1 + \frac{\phi}{\phi_m}q + \frac{1}{2}(q^2+q)(\frac{\phi}{\phi_m})^2 + ...$ When a suspension is diluted, ϕ is small compared to ϕ_m, the value of the successive terms decrease rapidly and the error induced by ignoring all but the first and second term is small. This gives that $(1 - \frac{\phi}{\phi_m})^{-q} \simeq 1 + \frac{\phi}{\phi_m}q$ can be considered to be a good approximation. When comparing this latter expression with Eq. 5.1 we see that $\frac{q}{\phi_m} = 2.5$ or as $q = [\eta]\phi_m$, we find that $[\eta] = 2.5$.

5.2.1 Rheological modelling for well cementing

Many equations have been introduced for the purpose of modelling the rheological behaviour of oil well cement suspensions. What they have in common is that they are all time independent. They vary from simple equations describing a linear relation between shear rate and shear stress to the more complex equations able to describe shear dependent relations.
A much used model in the oil cementing industry is the Bingham model:

$$\sigma = \sigma_y + \eta_p \, \dot{\gamma} \tag{5.5}$$

Here σ is the shear stress, σ_y is the yield stress, η_p is the plastic viscosity and $\dot{\gamma}$ is the shear rate. The use of the Bingham model is based on the shear stress measured at two different shear rates, this gives a straight line with a constant slope which is defined as the plastic viscosity. The stress value at zero shear rate is defined as the yield stress or yield point.
Another rather simple model is the power law model:

$$\sigma = k\,\dot{\gamma}^{n} \tag{5.6}$$

Here k is called the consistency index which is proportional to the apparent viscosity of a power law fluid and n is called the power law index, quantifying the degree of non-Newtonian behaviour. This model has been found to be able to describe the shear thinning behaviour of a variety of cementitious suspensions, but in contrast to the Bingham model it does not predict any yield point.
A more complex model much in use is the Herschel-Bulkley model:

$$\sigma = \sigma_y + k\,\dot{\gamma}^{n} \tag{5.7}$$

As can be seen from Eq. 5.7 this is a model that combines Eq. 5.5 and 5.6. This model is able to both predict a yield point and describe a power law behaviour.

5.2.2 The Quemada model

As basis for the rheological modelling related to the work leading up to this dissertation a model proposed by Quemada [3] in 1998 has been used [VII,VIII,X]. This model is described by Eq. 5.8 and it has been found suitable for describing the behaviour of shear thinning suspensions. The model is based on the K-D-model given by Eq. 5.2. With this model Quemada tries to account for inter-particle forces in both dilute and concentrated suspensions. The model proposed is given by:

$$\eta = \eta_\infty \left[\frac{1+\Gamma^p}{\chi+\Gamma^p}\right]^2 \tag{5.8}$$

Here η_∞ is the limiting steady state viscosity as $\Gamma \to \infty$. Γ is a dimensionless shear variable, either expressed in terms of the shear rate, $\Gamma = (\dot{\gamma}\ /\ \dot{\gamma}_c)$ or the shear stress, $\Gamma = \sigma/\sigma_c$, using a characteristic shear rate γ_c or stress σ_c

respectively. According to Quemada [3] the choice between these two forms of Γ will be dictated by the type of rheometer used for measurements and not, as was wrongly stated in Paper VII, the particle concentration of the suspensions. Further, $\dot{\gamma}_c = t_c^{-1}$ where t_c is a characteristic time required for dimensional homogeneity. The exponent p should be less than one and has been found experimentally to be close to 0.5 for colloidal dispersions [3]. The rheological index χ in Eq. 5.8 is a function of the packing fraction, ϕ, defined by [3]:

$$\chi = \chi(\phi) = \frac{1 - \frac{\phi}{\phi_0}}{1 - \frac{\phi}{\phi_\infty}} \equiv \left(\frac{\eta_\infty}{\eta_0}\right)^{\frac{1}{2}} \tag{5.9}$$

This rheological index depends on the limiting maximum packing, ϕ_m, at $\Gamma \to \infty$ and $\Gamma \to 0$ respectively, defined by:

$$\phi_\infty = \frac{\phi_m}{1 + CS_\infty} \quad and \quad \phi_0 = \frac{\phi_m}{1 + CS_0} \tag{5.10}$$

where C is a compactness factor and S is a structural variable. Both factors will be further discussed in Sect. 5.2.3. The packing fractions, ϕ_∞ and ϕ_0, are also involved in the corresponding steady state limiting viscosities, η_∞ and η_0:

$$\eta_\infty = \eta_F \left(1 - \frac{\phi}{\phi_\infty}\right)^{-2} \quad and \quad \eta_0 = \eta_F \left(1 - \frac{\phi}{\phi_0}\right)^{-2} \tag{5.11}$$

5.2.3 From the K-D model to the Quemada model

Prior to presenting how the K-D model forms the basis for the Quemada model, the concept of effective volume fraction, EVF, has to be introduced. This is a concept used by Quemada [3] as a basis for his rheological modelling and thus, a further understanding is needed.

Normally the term volume fraction is used when describing the amount of particles contained in a suspension. But when wanting to relate this to the degree of dispersion of the particles in a suspension, the term EVF is much in use. To explain the term EVF, one starts with the concept of a structural unit, SU. An SU is an aggregate of smaller particles of various sizes that stick together due to surface forces. The space between the particles in the SU is filled with the suspending fluid and this fluid becomes a part of the SU. The result is a reduction of the EVF of the continuous phase and an increase of the EVF of the particles.

Furthermore, under steady shear flow conditions the SUs are considered to have a shear dependent mean radius and to be approximately spherical in shape. This implies that a complex fluid can be considered as a roughly mono-disperse suspension. The shear thinning behaviour many times encountered for particle suspensions, going from low to moderate shear rates, can thus be accounted for by the increase in the EVF of the suspending fluid due to the shear induced reduction of the SUs' size and the consequent release of locked up fluid.
Further, to complete the description of the term EVF, the concept of individual flocs, IFs, is introduced. The IFs consist of small irreducible aggregates and it is assumed that some of the IFs have to remain free and are not to be included in the SUs.
This model proposed by Quemada [3], based on a structure consisting of almost monodisperse aggregates built up of SUs and IFs differs in that respect from the model proposed by Hattori and Izumi [25], used for cementitious suspensions [26], as the latter model is based on individual particles building a structure of chains and where the connections between the particles are formed due to inter-particle collisions.
According to Quemada [3] stabilized suspensions are only approximately described as hard sphere (HS) systems, depending on the interaction potential. However, in the case of a repulsive potential, often superposed to an attractive potential which reduces the interaction range, one can introduce an effective radius r_{eff} which defines the equivalent HS radius. This HS-approximation allows for using the K-D-equation after changing ϕ into an EVF:

$$\phi_{eff} = \frac{4\pi}{3} N r_{eff}^3 = \left(\frac{r_{eff}}{r}\right)\phi \tag{5.12}$$

the K-D-equation, Eq. 5.2 thus becomes:

$$\eta_r = \left(1 - \frac{\phi_{eff}}{\phi_m}\right)^{-q} \tag{5.13}$$

Eq. 5.13 has often been used in the form of the K-D equation, i.e. with $q = [\eta]\phi_m$ and using ϕ_{eff} defined from Eq. 5.12. But this gives that only the barrier, either steric or electrostatic, of the stabilizing potential is taken into account. Thus, Eq. 5.12 is found not to be sufficient in the presence of an attractive potential strong enough to promote particle clustering, i.e. when the dispersion should be described as a suspension of clusters. Nevertheless such a structural feature leads to an important change in the above-defined EVF concept. Extension of the HS-approximation to complex fluids directly results from including the formation of SUs in the model. This leads to a simple description of these fluids

as suspensions of SUs.
The size distribution of SUs is expected to be narrowed under flow conditions and centered on a mean size $\overline{R}(\Gamma)$ due to the shear forces acting on the SUs. The shear forces together with collisions between the SUs are expected to result in a more spherical shape of the SUs. However, as some amount of the suspending fluid is immobilized inside the SUs, there is a need to define a ratio, φ_n, as the volume of solids inside an SU to its total volume. This ratio defines the compactness of the SUs. The effective radius of an SU consisting of n particles with a radius of r thus becomes:

$$R_{eff} = \left(\frac{nr^3}{\varphi_n}\right)^{\frac{1}{3}} \tag{5.14}$$

Defining a mean compactness, φ, gives the relation between the total EVF and the true volume fraction ϕ by:

$$\phi_{eff} = \phi/\varphi \tag{5.15}$$

where $\phi_{eff} > \phi$ as $\varphi < 1$. However, the EVF definition in Eq. 5.15 may appear rather restrictive, so by also incorporating the term of IFs in Eq. 5.15, leads to a generalized definition of a suspension composed of SUs and IFs in dynamical equilibrium under steady flow conditions. The EVF of the suspension of SUs and IFs becomes:

$$\phi_{eff} = \phi_I + \phi_{Aeff}, \tag{5.16}$$

where ϕ_I is the volume fraction of the IFs and $\phi_{Aeff} = \phi_A/\varphi$ is the effective volume fraction of the SUs. Now we can write Eq. 5.16 as:

$$\phi_{eff} = \phi - \phi_A + \frac{\phi_A}{\varphi} = \left[1 + \frac{\phi_A}{\phi\varphi} - \frac{\phi_A}{\phi}\right]\phi \tag{5.17}$$

and by introducing the structural variable, $S = \phi_A/\phi$ defined as the aggregated fraction, or the total number density of primary particles contained in SUs, Eq. 5.15 becomes:

$$\phi_{eff} = [1 + CS]\phi \tag{5.18}$$

where $C = \varphi^{-1} - 1$ is a compactness factor directly related to the mean compactness, φ, of SUs.

To describe the structure kinetics there is a need for introducing the mean relaxation times, t_A for the aggregation of SUs and t_D for the destruction of the SUs. The change with time of the number of aggregated particles can then be written as:

$$\frac{dS}{dt} = \kappa_A(S_0 - S) - \kappa_D(S - S_\infty) \tag{5.19}$$

where $\kappa_A = t_A^{-1}$ and $\kappa_D = t_D^{-1}$ are shear dependent kinetic constants of formation and rupturing of SUs. S_0 and S_∞ are the limits of S at very low and very high shear, $\Gamma << 1$ and $\Gamma >> 1$ respectively. The steady state solution of Eq. 5.19, i.e. when $dS/dt = 0$ and $S = S_{eq}$, is given by:

$$S_{eq} = \frac{S_0 + S_\infty\theta}{1 + \theta} \tag{5.20}$$

Where θ is defined by

$$\theta = \kappa_D/\kappa_A = t_A/t_D = f(\Gamma) \tag{5.21}$$

This solution corresponds to the equilibrium structure the system reaches under constant shear, characterized by Γ.
The last step in modelling which concerns the relation between viscosity and structural variable, $\eta = f(S)$, involves a more original part in using the new EVF concept. From Eq. 5.13 we have $\eta = \eta(\phi_{eff})$ and from Eq. 5.18 we have that $\phi_{eff} = \phi_{eff}(S)$. Thus by inserting Eq. 5.18 into Eq. 5.13 we get:

$$\eta_r = \left[1 - \frac{1 + CS}{\phi_m}\phi\right]^{-q} \tag{5.22}$$

This gives, according to Quemada [3], that a one-to-one relation is automatically obtained, which describes the non-Newtonian viscosity under steady conditions, $\Gamma = constant$. Using the steady state solution $S_{eq} = S(\Gamma)$ of the kinetic equation results into $\eta(S_{eq}) = \eta(\Gamma)$. More precisely, inserting Eq. 5.20 into Eq. 5.22 leads to:

$$\eta_r = \left\{1 - \left[1 + \frac{C(S_0 + S_\infty\theta)}{1 + \theta}\right]\frac{\phi}{\phi_m}\right\}^{-2} \tag{5.23}$$

Here the exponent q of Eq. 5.22 has been set equal to 2, based on results from

a phenomenological study presented by Quemada in 1977 [27] concerning the viscosity of concentrated suspensions. Further, Eq. 5.23, when displayed step by step will lead to:

$$= \left\{ 1 - \left[1 + \frac{CS_0}{1+\theta} + \frac{CS_\infty \theta}{1+\theta} \right] \frac{\phi}{\phi_m} \right\}^{-2}$$

$$= \left\{ \phi_m - \phi - \frac{CS_0 \phi}{1+\theta} - \frac{CS_\infty \theta \phi}{1+\theta} \right\}^{-2}$$

$$= \left\{ \frac{(1+\theta)\phi_m - (1+\theta)\phi - (CS_0 - CS_\infty \theta)\phi}{1+\theta} \right\}^{-2}$$

$$= \left\{ \frac{\phi_m - \phi - CS_0\phi + (\phi_m - \phi - CS_\infty \phi)\theta}{(\phi_m - \phi - CS_\infty \phi)(1+\phi)} \right\}^{-2}$$

$$= \left\{ \frac{(\phi_m - \phi - CS_0\phi)/(\phi_m - \phi - CS_\infty \phi) + \theta}{1+\theta} \right\}^{-2}$$

$$= \left\{ \frac{1+\theta}{[1-(1+CS_0)\phi/\phi_m]/[1-(1+CS_\infty)\phi/\phi_m] + \theta} \right\}^{2} \qquad (5.24)$$

which with $\theta = \Gamma^p$ can be written in the form of the Quemada equation, Eq. 5.8:

$$\eta = \eta_\infty \left[\frac{1+\Gamma^p}{\chi + \Gamma^p} \right]^2$$

The use of this equation for rheological modelling of cementitious suspensions is presented in the following chapter.

Chapter 6

Main results and discussion

The rheological behaviour of cement suspensions are found to be shear-history-dependent and the amount of mixing energy used for mixing the suspensions is found to govern their behaviour when submitted to further testing in the laboratory. A fully dispersed suspension would, for a given particle type and volume fraction, result in a minima in the measured viscosity.
The main goal of the work has been to verify that the basis for using the Quemada model is present in cementitious suspensions and further, to show how the model could be used for predicting their rheological behaviour. The basis for using the Quemada model is the concept of a flocculated suspension where the degree of flocculation is shear dependent and further, to enable the particles in a suspension to approach each other and form flocs their repulsive electrostatic forces must be rather low.

6.1 Mixing energy

To be able to evaluate cement suspensions it is necessary to understand the effect of mixing energy on their performance. The absorbed mixing energy has been found to both vary and to have an impact on measured rheology data of the suspensions.

6.1.1 Mixing of cement suspensions

The amount of mixing energy induced during the high speed mixing of cement suspensions was investigated [I]. One of our main objectives was to compare our results with that of Orban, Parceveaux and Guillot [11, 12], who in 1986

introduced the term of specific mixing energy, SME. The SME was suggested to be used in the oil industry as a basis for a dimensionless SME of unity when relating other inputs of mixing energy. The value suggested to be used for this SME was 5.5 kJ/kg of suspension. This was based on their measurement of the amount of mixing energy absorbed during the 35 seconds of high speed mixing performed in accordance with API [6]. This value was measured on a neat Class G suspension having a w/c ratio of 0.44 by weight. The value of the SME has been confirmed through measurements [I]. However, we found that the use of such a term would require the input of mixing energy to be measured for all other suspensions as well, as the input of mixing energy in the high speed mixer was found to be both a function of the viscosity of the suspension and also of the type of propeller blade used in the high speed mixer. The amount of mixing energy induced by various types of propeller blades were also investigated [I]. This was due to the fact that the type of propeller blade to be used for high speed mixing was not given in the 1990 version of the API Standard [6] and that there existed various types of propeller blades on the market which were in frequent use. This variable related to the high speed mixing has later been removed as the 2005 version of the API Standard [14] now also states the type of propeller blade to be used in the high speed mixer.

6.1.2 Consistometer conditioning

Prior to any other testing than the thickening time, the suspension also experience 20 minutes of low speed mixing in the atmospheric consistometer. The input of mixing energy in the atmospheric consistometer during these 20 minutes was found to be 0.41 kJ/kg for a neat Class G suspension having a w/c ratio of 0.44 by weight and measured at a temperature of 20°C [II]. This input was calculated based on the torque measured in the consistometer shown in Fig. 6.1. This result in an additional input of mixing energy to the suspension of approximately 7.5% when compared with the value given for the SME. The input of mixing energy in the atmospheric consistometer was not investigated by Orban et al. [11, 12]. It is also expected that in this apparatus, the input of mixing energy will be directly related to the viscosity of the suspension and thus it should be measured.
During our work the original torque recording device of the atmospheric consistometer was replaced by a more sensitive load cell [II]. Thus, the measurements shown in Fig. 6.1 of the consistency development is recorded by this new load cell. Consequently we were able to register in more detail information concerning the development of the suspensions during testing in the atmospheric

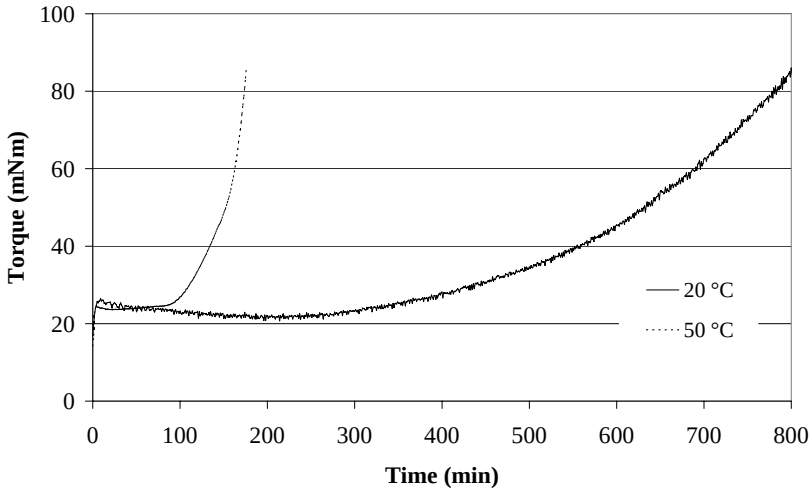

Figure 6.1: *Relation between time and torque measured at 20 °C and 50 °C in an atmospheric consistometer on a neat Class G slurry with a w/c ratio of 0.44 by weight. [II]*

consistometer.

For the suspensions shown in Fig. 6.1, we found that after a relatively short initial period, lasting only a few minutes, of increasing torque there followed a relatively long period of decreasing torque before the final onset of thickening started. This period of measured decrease in torque was found to last for more than 200 minutes for the neat Class G suspension tested at a temperature 20°C. This decrease in consistency is expected to reflect a reduction in the viscosity also found to appear, although at somewhat earlier times, for suspensions having a w/c ratio of 0.38 [I]. Further, the torque exerted on the stationary paddle in the consistometer has been found to be highly influenced by particle size and solid fraction [I, II]. A decrease in particle size and an increase in solid fraction both results in a marked reduction in thickening time. The term being used as it was reported that the consistency measurements in the atmospheric consistometer [I] was not found to give the setting time of the suspensions but rather the time for a viscous thickening to appear. Thus, it was concluded that another criteria such as the onset of thickening should be used instead of setting time.

6.1.3 Mixing energy and particle dispersion

In Fig. 6.2 is shown a picture of cement particles in a suspension consisting of neat Class G cement having a w/c ratio of 0.44 by weight. The picture was taken using a Scanning Electron Microscope, SEM, and after mixing in accordance with API [6, 14] and prior to any further measurements. The picture shows the

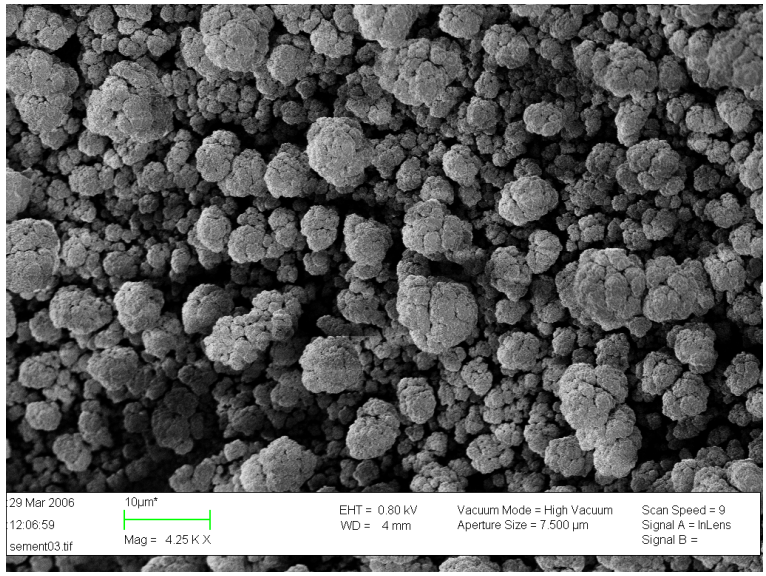

Figure 6.2: *A SEM picture of cement particles in a suspension of Class G cement. The suspension was mixed in accordance with API [6, 14] prior to quenching in liquid nitrogen. [IX]*

surface of a wet suspension quenched in liquid nitrogen prior to placement in the SEM. In the picture the water at the surface of the suspension has evaporated inside the SEM chamber due to the electron beam, but water can still be seen forming the darker "shadows" between and beneath the particles. The cement particles are found to form aggregates and the largest aggregates shown are found to have a diameter of approximately 10 μm whereas the individual cement particles seem to be 2 - 3 μm.
Based on density measurements [IX, X], it was also found that the particle aggregates pictured in Fig. 6.2 still contained air, which was found to increase the particle volume fraction by approximately 2 - 3% [IX, X]. The content of

air implies that the surface of the particles has not been fully hydrated. This we find supports the idea that the particles are still not fully dispersed after the mixing carried out in accordance with API [6, 14].
The presence of aggregated cement particles was also confirmed [IX], when prior to the rheological measurements, shearing for one minute at a relatively high shear rate of 1022 s^{-1} in the rheometer was needed in order to obtain stable readings at the highest reported shear rate of 500 s^{-1}. This additional shearing was found to both reduce the viscosity and to remove most of the air from the suspension. This is expected to be due to an improved dispersal of the particles [IX, X]. However, this additional shearing is not in accordance with the recommendations of API [6, 14].

6.1.4 Summary of mixing energy

The amount of energy applied for mixing the cement suspensions in accordance with API [6, 14], prior to any laboratory measurements, has been found both to vary [I] and to be insufficient to fully disperse the cement particles in the water [IX, X]. This is expected to reduce the reproducibility of the measurements for cement suspensions.

6.2 Electrostatic forces in cementitious suspensions

The inter-particle forces that we have been measuring in suspensions containing pure cement or cement combined with various types of cementitious materials, have been their electrostatic surface charges or zeta-potentials. The effect of these potentials or surface charges on the suspensions is presented in the following sections.

6.2.1 Zeta-potentials measured on cement particles

The zeta-potentials of the cement particles in the suspensions we have measured were always within the range of ±11 mV [II, IV, VII, VIII]. For these measurements we used the AcousoSizer as described in Sect. 4.2.5. The measurements were carried out on concentrated suspensions, consisting of neat Class G cement having a w/c-ratio of 0.44 by weight, which gives an approximate solid volume fraction of 0.41. The value of ±11 mV is rather low when compared with the values of ±60 - 80 mV needed to obtain stable dispersions, according to a rule of thumb given by Ney [28]. The absolute values of the zeta-potentials

are found to be in agreement with the values reported in the literature for various types of cement. In a study Nägele [18, 29, 30, 31], using the technique of micro-electrophoresis described in Sect. 4.2.3, reported that the zeta-potentials of Portland cements normally lie between ±30 mV and that the zeta-potential decreases in absolute value with increasing concentration. Yang, Neubauer and Jennings [32] also reported that the zeta-potential of cement is rather low. Using the technique of electrophoretic light-scattering, they found the zeta-potential

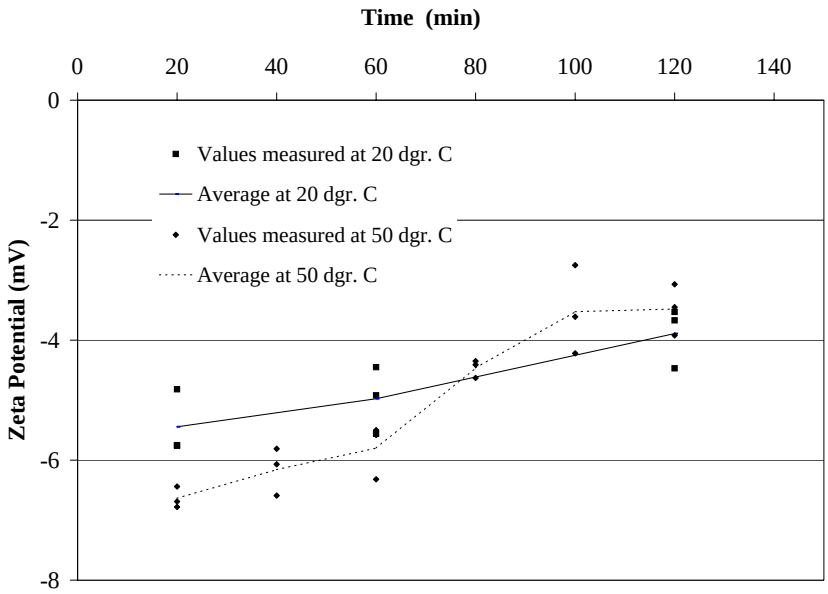

Figure 6.3: *Relation between time of agitation in an atmospheric consistometer and zeta-potential of the cement particles as measured by an AcoustoSizer [II].*

of Portland cement to lie between ±20 mV. Both Nägele and Yang et al. used diluted suspensions for their measurements.
The effect of time, temperature and continuous mixing on the development of the zeta-potential was also measured and the effect is shown in Fig. 6.3. Here it was found that the zeta-potential decreases as a function of time and continuous mixing and increases as a function of temperature when the temperature of the suspension was increased from 20°C to 50°C. However, at this elevated temperature the decrease in zeta-potential as a function of time and mixing was

more rapid than at 20°C, as can be seen from Fig. 6.3. As a result the absolute value of the zeta-potential measured after 60 minutes of continuous mixing at a temperature of 50°C was found to be lower than when mixed for 60 minutes at 20°C.

6.2.2 The zeta-potential of silica particles

The zeta-potentials of both crystalline silica flour and amorphous micro silica particles were also measured [IV, V]. The silica flour was measured to have a rather low zeta-potential in absolute value. It was found to be approximately -10 mV. This was measured on a suspension containing 19% by volume of silica flour.
The micro silica, on the other hand was found to have a high negative zeta-potential. It was measured to be -156 mV [IV] on a suspension containing approximately 3.3% by volume of micro silica. This large difference in measured zeta-potential of the silica particles is expected to reflect their difference in structure, one being crystalline and the other amorphous. For the amorphous micro silica the effect of increasing the solid volume fraction was a reduction in the zeta-potential. The zeta-potential was measured to be -49.1 and -42.7 mV for two samples containing 31 and 32% by volume of micro silica, respectively, and obtained from different suppliers [V].

6.2.3 The zeta-potential of manganese tetra oxide

The zeta-potential of manganese tetra oxide or Micromax particles were measured to be -1.55 mV in distilled water [VIII, X]. When suspended in cement-filtrate, ie. water containing only ions dissolved from cement, the zeta-potential changed to +6.8 mV. This reversal of sign and increase in absolute value of the zeta-potential is expected to be due to the adsorption of dissolved Ca^{+2} ions from the cement-filtrate.

6.2.4 The zeta-potential of mixed suspensions

Electroacoustics were also used to monitor the effect of adding silica and Micromax particles to cement suspensions [IV, V, VIII]. Because it is the net mass transfer that generates the sound waves detected with this measuring technique, the measured data needs to be interpreted with caution. The zeta-potential measured in a blended suspension is expected to be an averaged value, dependent on both the specific densities of the particles, their individual potential and their relative concentration in the suspension.

The effect of partly replacing the cement with crystalline silica flour and amorphous micro silica, or a combination of both, was measured [IV]. The adding of silica flour to the cement suspension did not result in any measurable change in the zeta-potential. This was measured on a suspension having a solid volume fraction of 0.44 and where approximately 13% by volume of the particles consisted of silica flour.
The effect of adding micro silica resulted in a slight reduction in the absolute value of the zeta-potential but it was still negative [IV]. This was measured on a suspension with a solid volume fraction equal to 0.424, where approximately 6% by volume of the particles consisted of micro silica.
The effect of adding manganese tetra oxide to the cement suspension also resulted in a slight reduction in the zeta-potential, from -10.7 mV measured on a neat cement suspension to -9.4 mV [VIII]. These measurements were done on a suspension containing 10% by volume of manganese tetra oxide and where the w/c-ratio of both suspensions were kept the same.

6.2.5 Summary of electrostatic forces

We have confirmed that the electrostatic repulsive forces of the cement particles and cementitious particles mixed with cement, are low in absolute value, and that they are too low to hinder flocculation to take place due to the attractive van der Waals forces. Further, we found that the cement particles dominate the development of the zeta-potentials when other materials are added to the cement in the suspensions. This is assumed at least for our suspensions where the volume fraction of the cementitious particles are limited to 13%. This is expected to be due to Ca^{2+} ions which readily dissolve from the cement particles into the water-phase of the suspensions. These ions are adsorbed on the surface of the initially negatively charged cementitious particles, making them less negative or even positive. As a whole, the repulsive electrostatic forces in cement suspensions were found to be low and according to Yang et al. [32], too low to hinder a flocculation of the particles in the suspensions.

6.3 Rheological modelling

The model proposed by Quemada [3] for rheological modelling of concentrated suspensions, has been applied for modelling cementitious materials used for well cementing. This is a model that tries to include the development of the "micro structure" in concentrated suspensions. The basic idea behind our work was to see if this model would be able to predict the rheological behaviour of cementitious suspensions, especially at low shear rates.

6.3.1 The practical approach to modelling

The applicability of the model proposed by Quemada [3] was investigated using two different approaches [VII, VIII, X]. For the rheological index χ, given by Eq. 5.9, Quemada states an identity between the particle packing relations and the viscosity relations at high and low shear respectively, requiring that an approach to obtain the index either through variations of the limiting viscosities or the packing should be equal. Thus, the model was tested out by obtaining the rheological index from variations in the limiting viscosities [VII]. Thereafter, the index was studied by varying the particle packing fractions [VIII, X].

6.3.2 Suspensions used for modelling

In a first approach to modelling we used rheological data obtained from three different suspensions [VII]. One suspension consisted of Class G clinker having a solid volume fraction of 0.419. The second consisted of neat Class G cement having a solid volume fraction of 0.408 and the third consisted of micro silica having a solid volume fraction of 0.311.
In both the second and the third approach to modelling our three suspensions used were based on the same formulations [VIII, X]. One was a neat Class G suspension having a w/c ratio by weight of 0.44 giving a solid volume of 0.41. In the other two suspensions the Class G cement was partly replaced by approximately 10% by volume of Micromax. In one of these latter suspensions the solid volume fraction was kept constant at 0.41 resulting in an increased w/c ratio of 0.49 in the other the w/c ratio was kept constant at 0.44 resulting in an increased solid volume fraction of 0.44.

6.3.3 Variable parameters and restrictions used for modelling

A method of determining the value of the rheological index χ given by Eq. 5.9, is by inserting values obtained for the solid volume fraction, ϕ, and the limiting maximum packing fraction, ϕ_m [X]. The latter being related to χ through Eq. 5.10. The parameters used in this approach together with their limiting values are shown in Table 6.1.
From Table 6.1 it can be seen that the solid volume fraction ϕ, of the cementitious suspensions was allowed to vary in the modelling. This was due to two main factors, one being the amount of chemically reacted water and the other the amount of air found to still adhere to the particles when the rheological measurements commenced [IX, X]. The amount of chemically reacted water was found to increase the solid volume fraction by approximately 2.1% at the

Table 6.1: *Parameters and limiting values used when modelling a neat Class G cement suspension and two suspensions also containing Micromax [X].*

Suspension:	Neat Class G SG=1.91	Cement added Micromax SG=1.98	Cement added Micromax SG=2.03
Parameters:	Limitations used	Limitations used	Limitations used
Exponent, p	$0.01 \leq p \leq 0.99$	$0.01 \leq p \leq 0.99$	$0.01 \leq p \leq 0.99$
Characteristic time, t_c [s]	$511^{-1} \leq t_c \leq 3.1^{-1}$	$511^{-1} \leq t_c \leq 3.1^{-1}$	$511^{-1} \leq t_c \leq 3.1^{-1}$
Solid volume fraction, ϕ	$0.42 \leq \phi \leq 0.43$ $\phi < \phi_0 < \phi_\infty$	$0.42 \leq \phi \leq 0.43$ $\phi < \phi_0 < \phi_\infty$	$0.45 \leq \phi \leq 0.46$ $\phi < \phi_0 < \phi_\infty$
Max packing fraction, ϕ_m	$0.69 \leq \phi_m \leq 0.74$	$0.71 \leq \phi_m \leq 0.74$	$0.71 \leq \phi_m \leq 0.74$
Volume fraction of particles contained in all the SUs when the shear rate $\rightarrow 0$, ϕ_{A0}	$\phi_{A0} \leq \phi$	$\phi_{A0} \leq \phi$	$\phi_{A0} \leq \phi$
Volume fraction of particles contained in all the SUs when the shear rate $\rightarrow \infty$, $\phi_{A\infty}$	$\phi_{A\infty} \leq \phi_{A0}$	$\phi_{A\infty} \leq \phi_{A0}$	$\phi_{A\infty} \leq \phi_{A0}$

start of the rheological measurements. The solid volume fraction ϕ was thus corrected for this increase and used as the lower limit for ϕ in our modelling. As density measurements indicated air to still be present in the suspensions after the initial preparations carried out in accordance with API, the volume fraction corrected for adhered air was used as an upper limit for the solid volume fraction ϕ. The volume increase of the particles due to adhered air was found to be approximately 2%.

The lower value of the maximum packing fraction ϕ_m used for the modelling was set equal to the maximum packing that we were able to obtain for the suspensions by use of a somewhat simplified packing technique [X]. In this packing technique a plastic syringe with a perforated piston and bottom were filled with the suspension in question. Holding back the particles by filters the water was then squeezed out using hand force only and at the same time vibrating the syringe. It was then reasoned that the true maximum packing would be higher than the packing that we were able to obtain using this method.

As the upper limit for maximum packing fraction we used the value of 0.74. This is the theoretical maximum packing fraction for a face centered packing of monodisperse spheres. It also reflects the shear dependent development of the SUs which form the basis for the Quemada model.

The two variables, ϕ_{A0} and $\phi_{A\infty}$, related to Eq. 5.10 through the structural variable S, being the volume fraction of particles contained in all the SUs as the

Table 6.2: *Parameters and limiting values used when re-modelling a neat Class G cement suspension and two suspensions also containing Micromax [VIII].*

Suspension:	Neat Class G w/c=44	Cement added 10% Micromax w/c=0.49	Cement added 10%Micromax w/c=0.44
Parameters:	Limitations used	Limitations used	Limitations used
Exponent, p	$0.01 \leq p \leq 0.99$	$0.01 \leq p \leq 0.99$	$0.01 \leq p \leq 0.99$
Characteristic time, t_c [s]	$511^{-1} \leq t_c \leq 34^{-1}$	$511^{-1} \leq t_c \leq 34^{-1}$	$511^{-1} \leq t_c \leq 34^{-1}$
Solid volume fraction, ϕ	$0.42 \leq \phi \leq 0.43$ $\phi < \phi_0 < \phi_\infty$	$0.42 \leq \phi \leq 0.43$ $\phi < \phi_0 < \phi_\infty$	$0.45 \leq \phi \leq 0.46$ $\phi < \phi_0 < \phi_\infty$
Max packing fraction, ϕ_m	$0.69 \leq \phi_m \leq 0.74$	$0.71 \leq \phi_m \leq 0.74$	$0.71 \leq \phi_m \leq 0.74$
Volume fraction of particles contained in all the SUs when the shear rate $\rightarrow 0$, ϕ_{A0}	$\phi_{A0} \leq \phi$	$\phi_{A0} \leq \phi$	$\phi_{A0} \leq \phi$
Volume fraction of particles contained in all the SUs when the shear rate $\rightarrow \infty$, $\phi_{A\infty}$	$\phi_{A\infty} \leq \phi_{A0}$	$\phi_{A\infty} \leq \phi_{A0}$	$\phi_{A\infty} \leq \phi_{A0}$
Volume fraction of particles contained in all the SUs, ϕ_A	$\phi_A \leq \phi_{A0}$ $\phi_A < \phi_{Aeff}$	$\phi_A \leq \phi_{A0}$ $\phi_A < \phi_{Aeff}$	$\phi_A \leq \phi_{A0}$ $\phi_A < \phi_{Aeff}$
Effective volume fraction of particles contained in all the SUs, ϕ_{Aeff}	$\phi_{Aeff} \leq \phi$	$\phi_{Aeff} \leq \phi$	$\phi_{Aeff} \leq \phi$

shear rate $\rightarrow 0$ and $\rightarrow \infty$ respectively, were restricted to be less or equal to ϕ. Furthermore $\phi_{A\infty}$ was restricted to be less or equal to ϕ_{A0} as increasing shear rates will tend to destroy the SUs.
The characteristic time, t_c, being the inverse of the characteristic shear rate, $\dot{\gamma_c}$, was restricted to the range of shear rates from 511 s^{-1} down to 3.1 s^{-1}. This range being in accordance with shear rates recommended by API [14], and also used when comparing the measured viscosity data and the viscosity data given by the model until a best fit was obtained. Thus, t_c was allowed to vary between 1.96 ms and 322.58 ms respectively.
To obtain a numerical value used for the the mean compactness, φ, it was, for this modelling, set equal to the solid volume fraction ϕ.
Finally, the exponent p of Eq. 5.9 was allowed to vary throughout the whole range of $0.01 \leq p \leq 0.99$ as an experimental adjustment to $0 < p < 1$.

As a result of the development concerning our modelling tool but also the dis-

Table 6.3: *Parameters and limiting values used when re-modelling a neat Class G cement suspension, a Class G clinker suspension and a Micro silica suspension [VII].*

Suspension:	Neat Class G	Class G clinker	Micro silica
Parameters:	Limitations used	Limitations used	Limitations used
Exponent, p	$0.01 \leq p \leq 0.99$	$0.01 \leq p \leq 0.99$	$0.01 \leq p \leq 0.99$
Characteristic time, t_c [s]	$511^{-1} \leq t_c \leq 5.1^{-1}$	$1020^{-1} \leq t_c \leq 1.49^{-1}$	$1020^{-1} \leq t_c \leq 5.1^{-1}$
Solid volume fraction, ϕ	$0.42 \leq \phi \leq 0.43$ $\phi < \phi_0 < \phi_\infty$	$\phi = 0.419$ $\phi < \phi_0 < \phi_\infty$	$\phi = 0.311$ $\phi < \phi_0 < \phi_\infty$
Max packing fraction, ϕ_m	$0.69 \leq \phi_m \leq 0.74$	$0.63 \leq \phi_m \leq 0.74$	$0.63 \leq \phi_m \leq 0.74$
Volume fraction of particles contained in all the SUs when the shear rate $\rightarrow 0$, ϕ_{A0}	$\phi_{A0} \leq \phi$	$\phi_{A0} \leq \phi$	$\phi_{A0} \leq \phi$
Volume fraction of particles contained in all the SUs when the shear rate $\rightarrow \infty$, $\phi_{A\infty}$	$\phi_{A\infty} \leq \phi_{A0}$	$\phi_{A\infty} \leq \phi_{A0}$	$\phi_{A\infty} \leq \phi_{A0}$
Volume fraction of particles contained in all the SUs, ϕ_A	$\phi_A \leq \phi_{A0}$ $\phi_A < \phi_{Aeff}$	$\phi_A \leq \phi_{A0}$ $\phi_A < \phi_{Aeff}$	$\phi_A \leq \phi_{A0}$ $\phi_A < \phi_{Aeff}$
Effective volume fraction of particles contained in all the SUs, ϕ_{Aeff}	$\phi_{Aeff} \leq \phi$	$\phi_{Aeff} \leq \phi$	$\phi_{Aeff} \leq \phi$

covery that slippage most probably had influenced the results of our earlier modelling [X], these data [VII, VIII] have been the subject of re-modelling. The results are presented as a part of the present dissertation. The restrictions used for this re-modelling are shown in Table 6.2 and 6.3.

In Table 6.2 the restrictions used are mainly the same as those shown in Table 6.1. This is due to the fact that the suspensions are the same. However, the labelling used when the suspensions were first presented has been kept as to avoid any confusion [VIII]. What has been changed is the range of shear rates used for obtaining the critical time t_c. Thus, for the re-modelling the range from 511 down to 34 s^{-1} were used. This because it was discovered, in retrospect [X], that the values measured at shear rates below 34 s^{-1} most likely had been influenced by slippage.

In addition, compared with the parameters listed in Table 6.1, two more parameters have been allowed to vary, this is the volume fraction of all the particles contained in all the SUs, ϕ_A, and their respective effective volume fraction, ϕ_{Aeff}. Both are restricted to be less or equal to the particle volume fraction,

ϕ, and ϕ_A is further restricted to be less than ϕ_{Aeff} as the mean compactness, $\varphi = \phi_A/\phi_{Aeff}$, should be less than unity.
In Table 6.3 the restrictions used for re-modelling of three suspensions are shown [VII]. One suspension consisted of neat Class G cement, one consisted of Class G clinker and the third suspension consisted of Micro silica. For these suspensions the shear rates used for obtaining the critical time, t_c, are the same as those presented in the original work [VII]. Although some of the data had been influenced by slippage, it was concluded that this was a minor issue and could be disregarded.
The particle volume fraction, ϕ, used for the neat Class G cement suspension was slightly changed from that used in the original modelling [VII] as it was allowed to vary within the same interval as the neat Class G cement of Table 6.1 and 6.2. For the other two suspensions we used the same particle volume fractions as those used in the earlier modelling [VII].
For maximum particle packing fractions, ϕ_m, we also used the values found for the neat Class G cement suspension presented in Table 6.1 and 6.2. For the other suspensions we allowed the maximum particle packing fraction to vary between 0.63 and 0.74. the first one representing the random close packing and the second representing the theoretical value of face centered cubic packing. The other limiting values used were the same as those presented in Table 6.2.

6.3.4 The results of modelling

By applying the Quemada equation, Eq. 5.8, on cementitious suspension and by using the restrictions mentioned under Table 6.1, we were able to show that the model predicts two similar and optimal solutions for each suspension [X]. These optimal solutions are shown in Figs. 6.4, 6.5 and 6.6 where the results are plotted as a function of viscosity against shear rate. In these figures the measured values are marked as points and the solutions obtained through the modelling, drawn as curves. The optimal parameters found for these curves are shown in Table 6.4. One of these optimal solutions was found to indicate both an upper and a lower plateau of the viscosity with respect to the shear rate, going through a shear thinning region in between. The upper plateau in this context, being a region of relatively low and constant viscosity at high shear rates as indicated by the curves to the right in the figures and a lower plateau consequently being a region of relatively high and constant viscosity at low shear rates as indicated to the left in the figures. For short these solutions were denoted as s-type of curves and further, they were found to indicate the non-existence of a yield stress for our suspensions. In the figures they are drawn as dotted lines. The other type of optimal solution found also indicated an upper plateau of the viscosity with

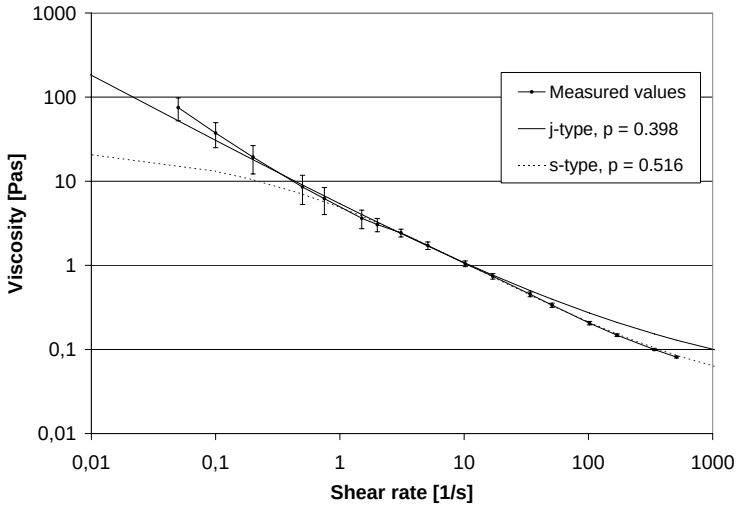

Figure 6.4: *Measured and modelled data for a neat Class G cement suspension having a SG of 1.91, a solid volume fraction of 0.41 and a w/c ratio of 0.44 by weight [X].*

Table 6.4: *Optimal parameters found when modelling our suspensions. The two optimal solutions found for each of the three suspensions are given. Included are also the limiting values of the viscosity as given by the model [X].*

Parameters	Neat Class G SG=1.91		Cement + Micromax SG=1.98		Cement + Micromax SG=2.03	
p	0.398	0.516	0.419	0.521	0.413	0.541
t_c	0.00196	0.00225	0.00196	0.00196	0.00196	0.00196
ϕ	0.43	0.43	0.43	0.42	0.45	0.45
ϕ_m	0.726	0.728	0.71	0.71	0.71	0.71
ϕ_{A0}	0.223	0.221	0.211	0.208	0.213	0.210
$\phi_{A\infty}$	0.113	0.097	0.118	0.101	0.133	0.111
R^2	0.999869	0.999905	0.999953	0.999899	0.999736	0.999940
η_0	2.4 MPas	26.3 Pas	2.4 MPas	59.2 Pas	2.7 MPas	61.6 Pas
η_∞	32.3 mPas	24.2 mPas	42.6 mPas	28.7 mPas	68.9 mPas	42.1 mPas

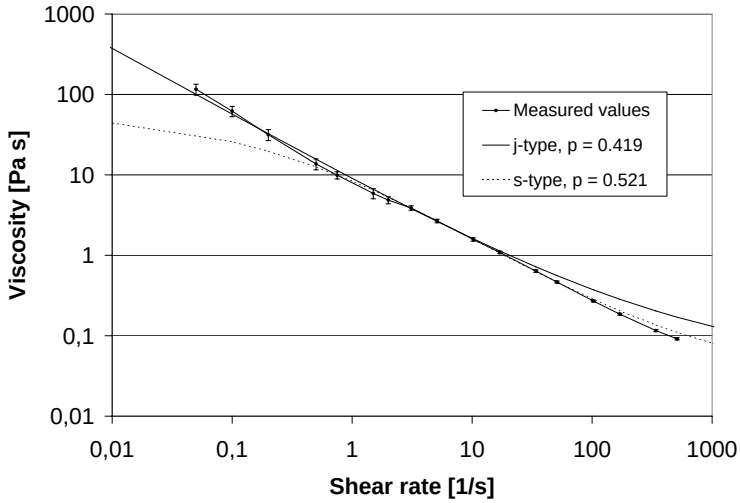

Figure 6.5: *Measured and modelled data for a Class G cement suspension where 11.4% by volume of the cement is replaced with Micromax®, having a SG of 1.98, a total solid volume fraction of 0.41 and a w/c ratio of 0.49 by weight [X].*

respect to the shear rate but this solution did not indicate the existence of a lower plateau. Instead a shear thinning region towards lower shear rates was indicated. For short these solutions were denoted as j-type of curves. Contrary to the s-type of curves, they do not exclude the existence of a yield stress for our suspensions. In the figures the j-type of curves are drawn as solid lines.
To better illustrate whether a yield stress is indicated or not by the two types of curves found for each suspension the results found for the neat Class G suspension and shown in Fig. 6.4, have been plotted in Fig. 6.7 as shear stress against shear rate. This figure we find shows more clearly that the j-type of curve indicates a yield stress while the s-type is found to indicate the non-existence of a yield stress. During our latest work the phenomenon of slippage was also encountered [X]. According to Coussot [33] the physical nature of wall slip remains somewhat open. However, it is generally assumed that wall slip is negligible when the roughness of the wall becomes much greater than the typical element size. Thus, the rotating cylinder in the coaxial configuration used for our latest measurements were changed from a smooth surface type to a type having a roughened surface [X]. In so doing the effect of slippage was reduced to a negligible level where it had either a small or no influence on the measured

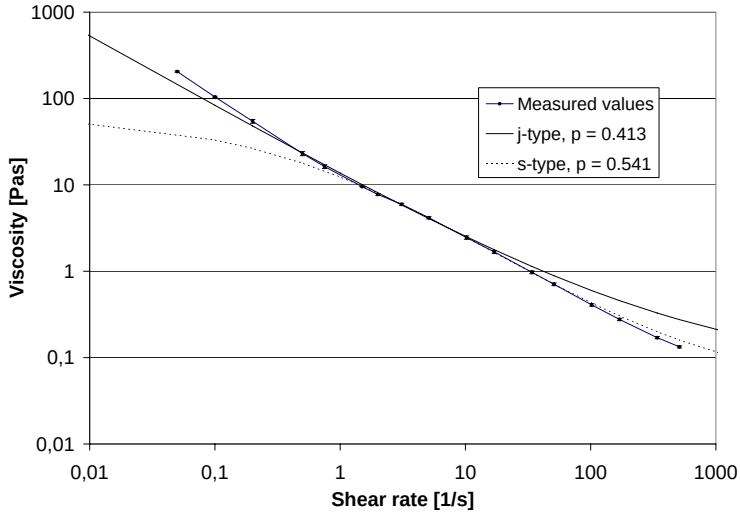

Figure 6.6: *Measured and modelled data for a Class G cement suspension where 10.3% by volume of the cement is replaced with Micromax®, having a SG of 2.03, a total solid volume fraction of 0.44 and a w/c ratio of 0.44 by weight [X].*

Table 6.5: *Optimal parameters found when re-modelling our suspensions. The two optimal solutions found for each of the three suspensions are given. Included are also the limiting values of the viscosity as given by the model [VIII].*

Parameters	Neat Class G w/c=0.44		Cement + 10% Micromax w/c=0.49		Cement + 10% Micromax w/c=0.44	
p	0.507	0.591	0.527	0.64	0.496	0.68
t_c	0.00199	0.00302	0.00196	0.00204	0.00196	0.00219
ϕ	0.43	0.42	0.43	0.43	0.458	0.45
ϕ_m	0.726	0.69	0.71	0.71	0.71	0.736
ϕ_{A0}	0.117	0.135	0.162	0.224	0.216	0.346
$\phi_{A\infty}$	0.045	0.061	0.071	0.098	0.114	0.200
R^2	0.999991	0.999994	0.999991	0.999926	0.999873	0.999994
η_0	2.4 MPas	20.7 Pas	2.3 MPas	15.5 Pas	3.4 MPas	10.1 Pas
η_∞	20.5 mPas	20.7 mPas	26.8 mPas	25.5 mPas	45.6 mPas	45 mPas
ϕ_A	0.115	0.111	0.142	0.144	0.187	0.129
ϕ_{Aeff}	0.405	0.328	0.387	0.32	0.405	0.233

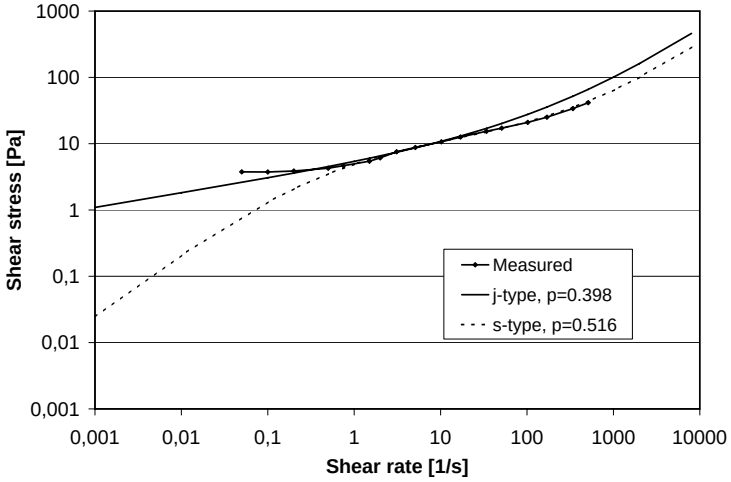

Figure 6.7: *Measured and modelled data for a neat Class G cement suspension having a SG of 1.91, a solid volume fraction of 0.41 and a w/c ratio of 0.44 by weight.*

values. Bearing this in mind, the measured values for all our suspensions presented in Figs. 6.4, 6.5, and 6.6 can be seen to have a minor local deviation from a smooth curve in the shear rate range from approximately 2 s^{-1} down to approximately 0.5 s^{-1} which could be interpreted to be caused by slippage. However, these values were not included and used as basis for our modelling [X].

It should also be mentioned that Guillot [34] reports that the decreasing and increasing values measured as a function of decreasing shear rates, here reflecting the values in the "slip region" and at shear rates in the region below, could be caused by sedimentation. But no sign of sedimentation was observed when inspecting the measuring cup after our measurements [X]. A more plausible interpretation of the build up of viscosity towards lower shear rates, below the "slip region", could be that the cement particles are, due to the relatively low shear rates, able to build up a structural network.

In Figs. 6.8 to 6.13 our re-modelling of the earlier work is presented [VII, VIII]. In these figures the result of the original modelling is also shown, bearing the legend "Old Quemada Modelling".

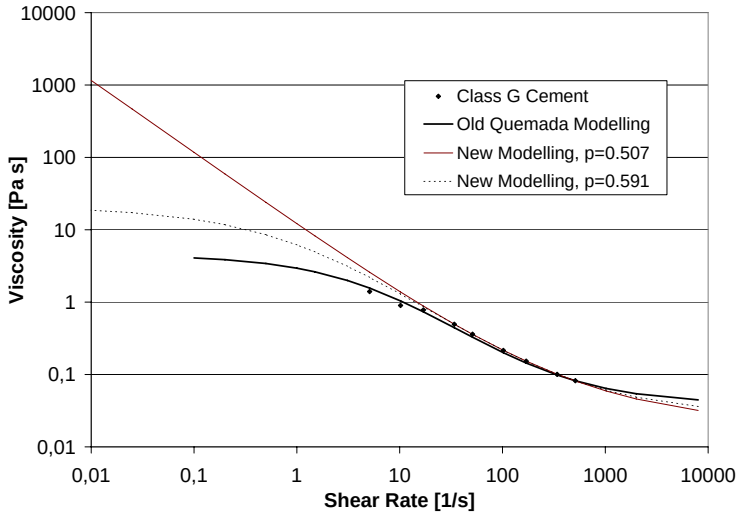

Figure 6.8: *Measured and modelled data for a neat Class G cement suspension having a solid volume fraction of 0.419 and a w/c ratio of 0.44 by weight [VIII].*

As mentioned, this re-modelling was found to be of interest both due to improvements in our modelling tool but also due to the fact that during our latest work we found that some of the measured data presented in the earlier work most likely had been influenced by slippage [X]. This slippage was found to occur at the lower shear rates with the result that the measured values reported for these shear rates tend to be lower than the actual values. In the figures the deviation found in the measured values from a linear development of the viscosity when going from higher towards lower shear rates, starting at the shear rate of approximately 34 s^{-1}, is interpreted to be due to the occurrence of slip. This is most clearly shown in Figs. 6.8, 6.9 and 6.10, but a slight deviation can also be found in Figs. 6.11, 6.12. Only for the Micro silica shown in Fig. 6.13 no apparent slippage can be detected in the measured values. This we find also to be reflected in the outcome of the original modelling as the optimal solutions found for the suspensions where slippage was indicated were of the s-type while the solution found for the Micro silica resulted in a curve of the j-type. The optimal parameters found in our re-modelling of the various suspensions are shown in Table 6.5 and 6.6.
As can be seen from the Figs. 6.8 to 6.13 when considering only the "Old Quemada Modelling" curves, the existence of two types of optimal solutions had also been found as a result of the earlier modelling [VII,VIII]. However, only

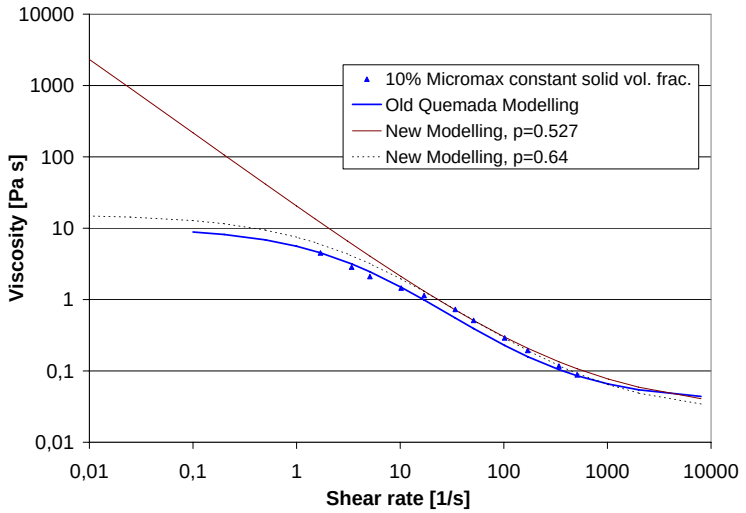

Figure 6.9: *Measured and modelled data for a Class G cement suspension added 10% Micromax® by volume, having a solid volume fraction of 0.419 and a w/c ratio of 0.49 by weight [VIII].*

one optimal solution was identified for each of the suspensions. From Figs. 6.8 to 6.13 it can be seen that the re-modelling resulted in two optimal solutions for each of the suspensions. One of the s-type and one of the j-type. Further, this is found to be in accordance with the two optimal solutions found and presented in Figs. 6.4, 6.5 and 6.6. The suspensions presented in Figs. 6.8, 6.9 and 6.10 are identical to the suspensions previously presented in Figs. 6.4, 6.5 and 6.6 respectively. However, due to the slippage found most likely having influenced the measured data presented in Figs. 6.8, 6.9 and 6.10, at low shear rates, only the viscosities measured at the six highest shear rates were used for the re-modelling.

When comparing the optimal parameters found for the re-remodelled suspensions, shown in Table 6.5, with the values obtained for the identical suspensions shown in Table 6.4 we find that the most notable difference is the value of the exponent p which for all the suspensions subject to re-modelling, have increased with an approximate value of 0.1. This we find mainly reflects the difference in the data obtained for the various identical suspensions. Although the values reported at the highest shear rates of 511 s^{-1} only differ by 2-3 mPAs when comparing the various identical suspensions shown in Figs. 6.4 to 6.10, the values at 34 s^{-1} differ more markedly and were always higher for the suspensions

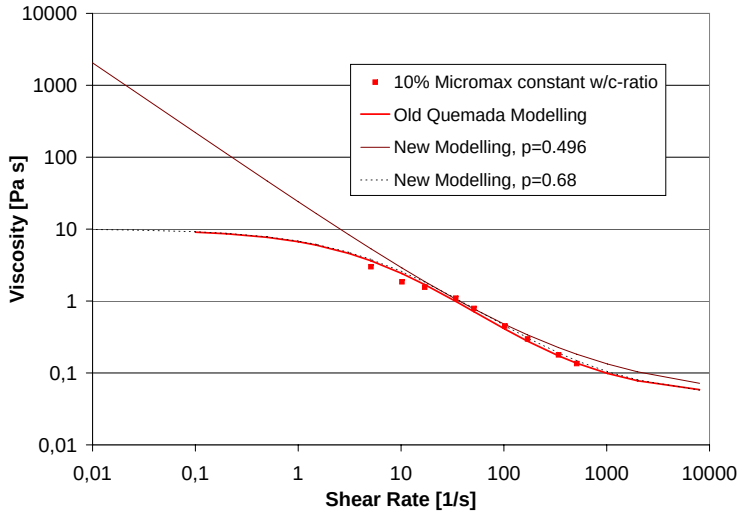

Figure 6.10: *Measured and modelled data for a Class G cement suspension added 10% Micromax® by volume, having a solid volume fraction of 0.442 and a w/c ratio of 0.44 by weight [VIII].*

Table 6.6: *Optimal parameters found when re-modelling our suspensions. The two optimal solutions found for each of the three suspensions are given. Included are also the limiting values of the viscosity as given by the model [VII].*

Parameters	Neat Class G		Class G clinker		Micro silica	
p	0.284	0.75	0.771	0.794	0.419	0.494
t_c	0.00196	0.00545	0.00915	0.00748	0.00778	0.01149
ϕ	0.428	0.43	0.419	0.419	0.311	0.311
ϕ_m	0.707	0.705	0.671	0.706	0.63	0.639
ϕ_{A0}	0.22	0.208	0.335	0.222	0.311	0.167
$\phi_{A\infty}$	0.113	0.114	0.183	0.11	0.090	0.065
R^2	0.996561	0.999993	0.999884	0.999866	0.999896	0.999945
η_0	2.9 MPas	1.58 Pas	2.3 MPas	9.2 kPas	1.5 kPas	6.1 Pas
η_∞	35.1 mPas	35.1 mPas	44.5 mPas	30.3 mPas	10.1 mPas	12.8 mPas
ϕ_A	0.18	0.183	0.225	0.179	0.19	0.148
ϕ_{Aeff}	0.408	0.407	0.394	0.412	0.384	0.429

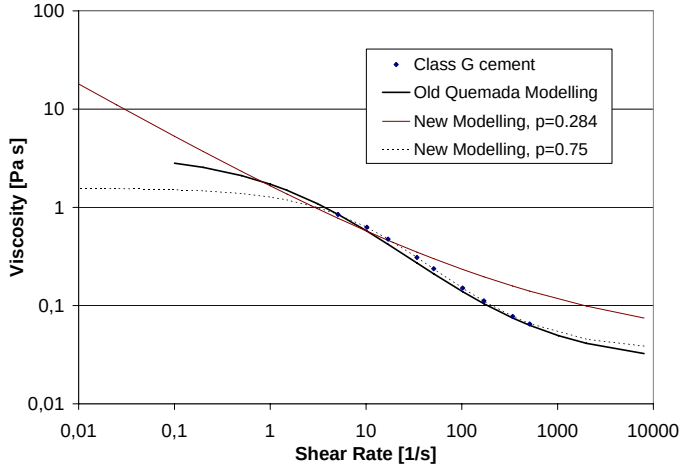

Figure 6.11: *Measured and modelled data for a neat Class G cement suspension having a solid volume fraction of 0.41 [VII].*

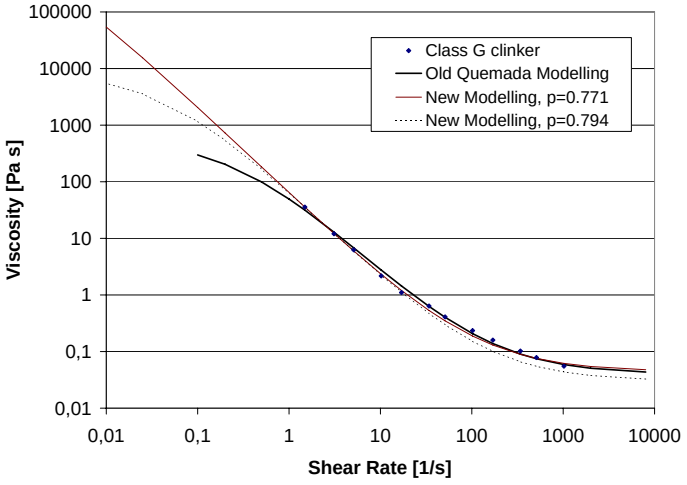

Figure 6.12: *Measured and modelled data for a Class G clinker suspension having a solid volume fraction of 0.419 [VII].*

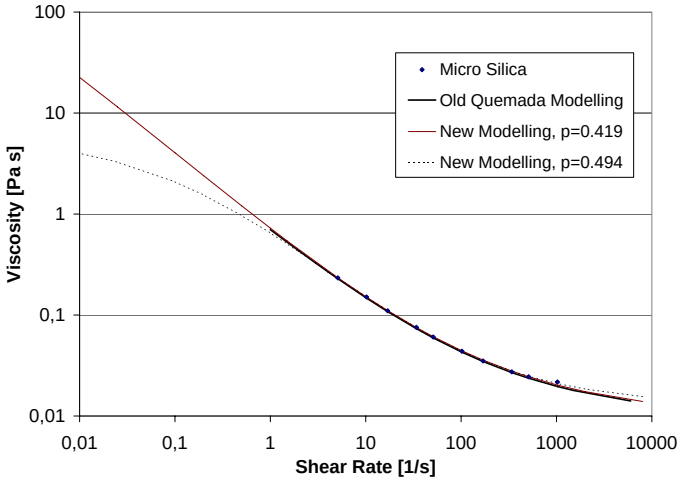

Figure 6.13: *Measured and modelled data for a Micro silica suspension having a solid volume fraction of 0.311 [VII].*

subject to re-modelling. For the neat Class G suspension shown in Fig. 6.8 the value measured at a shear rate of 34 s^{-1} was 42 mPas or 9.3% higher than that measured at the same shear rate for the neat Class G suspension shown in Fig. 6.4. For the suspension containing Micromax shown in Fig. 6.9 the value measured at a shear rate of 34 s^{-1} was 91 mPas or 14.3% higher than that measured at the same shear rate for the identical suspension shown in Fig. 6.5. For the suspension shown in Fig. 6.10 the value measured at a shear rate of 34 s^{-1} was 123 mPas or 12.7% higher than that measured at the same shear rate for the identical suspension shown in Fig. 6.6.
Whether the differences in the data sets are either due to the use of two different rheometers [VIII, X], both described in Sect. 5.1.1, equipped with different concentric configurations, or to the use of different batches of Class G cement could not be said. The Micromax particles used were from the same batch.

For the suspensions shown in Figs. 6.11, 6.12 and 6.13 all the measured viscosity data were used when re-modelling. This was decided as the effect of slippage on the measured values were considered to be minor for the data shown in Figs.6.11 and 6.12 and to be absent from the data shown in Fig.6.13. For these suspensions the optimal parameters found are presented in Table 6.6.
Again the "Old Quemada Modelling" curves shown in Figs. 6.11, 6.12 and 6.13 are the results of our earlier modelling [VII]. In this "old" modelling only four

parameters were allowed to vary. Two were the limiting viscosities, η_0 and η_∞ used in Eq. 5.9 to obtain a value for χ, the others were the characteristic time, t_c, to obtain Γ and the exponent p, all of Eq. 5.8.
When comparing the "Old Quemada Modelling" curves with the re-modelled curves of the same type, either the s-type, shown in Figs. 6.11 and 6.12 or the j-type shown in 6.13, we find that there is a relatively good agreement between the various curves. However, the j-type of curve resulting from the re-modelling and shown in Fig. 6.11, bearing the legend "New Modelling, p=0.284", were not found to compare well with the measured data. This is expected to be due to the use of data subject to slippage, data that we find most likely should have been omitted for this re-modelling. As mentioned earlier, the use of data influenced by slippage for our modelling will help in promoting the s-type of curves.

6.3.5 Summary of modelling

When modelling our suspensions we found that by varying the parameters involved, the model is able to predict two optimal solutions for each suspension. One solution, resulting in an s-type of curve, was found to give the best prediction of the rheological behaviour of our suspensions toward higher shear rates while the other solution, resulting in a j-type of curve, was found to give the best prediction of the rheological behaviour of our suspensions toward lower shear rates. Also, the j-type of curve was found to predict the existence of a yield stress.
However, care should be taken when choosing the rheological data used as a basis for the modelling of cementitious suspensions. In particular one should assure that the data used are not subject to slippage.

Chapter 7

Conclusion

The amount of mixing energy used for mixing cementitious suspensions prior to laboratory testing in accordance with API are found not to be sufficient to fully disperse the particles.

Through measurements we have confirmed that the surface forces encountered in cementitious suspension are low, too low to hinder flocculation of the particles.

The formation of shear-dependent aggregates of particles forming the basis for the rhehological model proposed by Quemada is present.

The Quemada modell has been found to be able to predict the rheological behavior of cementitious suspensions based on measurements carried in accordance with API Standard.

The Quemada modell predicts two optimal solutions for each suspension.

The solution predicting the existence of a yield stress has been found to give the best prediction of the rheological behaviour of cementitious suspensions towards lower shear rates.

Bibliography

[1] Hodne, H.,Wick, S.O., Jakobsen, R.A. and Saasen, A., "Comparative Study of Testing Methods for Cement pastes", Annual Transactions The Nordic Rheology Society, **5**, 129-134, (1997).

[2] Hodne, H., O'Hagan, A.B., Saasen, A. and Wick, S.O., "Effects of Shear History on the Viscosity and Gel Development of Oil Well Cement Slurries", Annual Transactions The Nordic Rheology Society, **6**, 51-54, (1998).

[3] Quemada, D., "Rheological modelling of complex fluids. I. The concept of effective volume fraction revisited", Eur. Phys. J. AP, **1**, 119-127, (1998).

[4] Lea, F.M., "The Chemistry of Cement and Concrete", 3rd edition, Edward Arnold Ltd. (1970)

[5] Michaux, M., Nelson, E.B. and Vidick, B., "Chemistry and Characterization of Portland Cement", in: Nelson, E. B. (Ed.), Well Cementing, Elsevier Science Publishers B.V., Developments in Petroleum Science 28, (1990)

[6] American Petroleum Institute, "Specifications for Materials and Testing for Well Cements", API Spec. 10, Fifth ed., Washington DC, July 1.,(1990).

[7] Nelson, E.B., Baret, J-F. and Michaux, M., "Cement Additives and Mechanism of Action", in: Nelson, E. B. (Ed.), Well Cementing, Elsevier Science Publishers B.V., Developments in Petroleum Science 28, (1990)

[8] Banfill, P.F.G., "The rheology of fresh cement and concrete - a review", Proc. 11th Int. Congress on the Chemistry of Cement, **1**, 50-62, (2003).

[9] Banfill, P.F.G. and Swift, D.S., "The effect of mixing on the rheology of cement-based materials containing high performance superplasticisers", Annual Transactions The Nordic Rheology Society, **12**, 9-12, (2004).

[10] van Kleef, R.P.A.R. and van Vllet, J.P.M., "Improving the Reliability of Cement-Setting-Time tests by Taking Into Account the Influence of Shear", SPE Drilling and Completion, SPE 20926, (1993).

[11] Orban, J., Parceveaux, P. and Guillot, D., "Influence of Shear History on the Rheological Properties of Oil Well Cement Slurries", 8th ICCCt, Rio de Janeiro, **6**, 243-247, (1986).

[12] Orban, J., Parceveaux, P. and Guillot, D., "Specific Mixing Energy: A Key Factor for Cement Slurry Quality", 61st Ann. Technical Conference and Exhibition of the Society of Petroleum Engineers, New Orleans, Oct.5-8., SPE 15578, (1986).

[13] Vlachou, P.-V. and Piau, J.-M., "The Influence of the shear Field on the Microstructural and Chemical Evolution of an Oil Well Cement Slurry and its Rheometric Impact", Cem. and Concr. Res., **27**, 869-881, (1997).

[14] American Petroleum Institute, "Recommended Practice for Testing Well Cements", API RP 10B-2/ISO 10426-2, First Edition, July, (2005).

[15] Israelachvili, J., "Intermolecular & Surface Forces", Academic Press, (1991).

[16] Hunter, R.J., "Foundations of Colloid Science", Volume I, Oxford University Press, (1993)

[17] Shaw, D.J.,"Introduction to Colloid and Surface Chemistry", Butterworths & Co. Ltd., London, (1980).

[18] Nägele, E., "The Zeta-Potential of Cement", Cem. and Concr. Res., Pergamon Press, Ltd., **15**, 453-462, (1985).

[19] Hunter, R.J., "Introduction to Modern Colloid Science", Oxford University Press, (1996).

[20] Hunter, R.J., "Review - Recent developments in the electroacoustic characterisation of colloidal suspensions and emulsions", Colloids and Surfaces, A: Physicochemical and Engineering Aspects, **141**, 37-65, (1997).

[21] O'Brien, R.W., Cannon, D.W., and Rowlands, W.N., "Electroacoustic Determination of Particle Size and Zeta Potential", J. Coll. Interface Sc., **173**, 406-418,(1995).

[22] Colloidal Dynamics, "AcoustoSizer, User's Manual", Colloidal Dynamics, Inc., 60 Alhambra Road, Suit 2, Warwick, Rhode Island 02886 USA, (1997).

[23] Barnes, H.A., Hutton, J.F. and Walters, K., "An Introduction to Rheology", Elsevier Science Publishers B.V., Rheology Series, 3, (1989)

[24] Asimov, I., "Understanding Physics", Barnes & Noble Books, II-109, (1993).

[25] Hattori, K. and Izumi, K., "A new viscosity equation for non-Newtonian suspensions and its application", in: Banfill, P.F.G.(Ed.), Rheology of Fresh Cement and Concrete, Chapmann and Hall, 83-92, (1991).

[26] Wallevik, J.E., "Rheology of Particle Suspensions, Fresh Concrete, Mortar and Cement Paste with Various Types of Lignosulfonates", PhD thesis, The Norwegian University of Science and Technology (NTNU), Trondheim, Norway, (2003)

[27] Quemada, D., "Rheology of concentrated disperse systems and minimum energy dissipation principle. I. Viscosity-concentration relationship", Rheol. Acta, **16**, 82-94, (1977).

[28] Ney, P., "Zeta-Potentiale und Flotierbarkeit von Mineralien", Springer-Verlag Wien, New York (1973).

[29] Nägele, E., "The Zeta-Potential of Cement, Part II: Effect of pH-Value", Cem. Concr. Res., **16**, 853-863, (1985).

[30] Nägele, E., "The Zeta-Potential of Cement Part III: The Non-Equilibrium Double Layer on Cement", Cem. Concr. Res., **17**, 573-580, (1987).

[31] Nägele, E. and Schneider, U., "The Zeta-Potential of Cement Part IV: Effect of Simple Salts", Cem. Concr. Res., **17**, 977-982, (1987).

[32] Yang, M., Neubauer, C.M. and Jennings, H.M., "Interparticle Potential and Sedimentation Behaviour of Cement Suspensions; Review and Results from Paste", Advn. Cem. Bas. Mat., Elsevier Sci., **5**, 1-7, (1997)

[33] Coussot, P., "Rheometry of Pastes, Suspensions, and Granular Materials: Applications in Industry and Environment", John Wiley & Sons, Inc., (2005).

[34] Guillot, D., "Rheology of Well Cement Slurries", in: Nelson, E. B. (Ed.), Well Cementing, Elsevier Science Publishers B.V., Developments in Petroleum Science 28, (1990)